

1 **Title:**

2 **Pancreatic stellate cells derived from human pancreatic cancer**
3 **demonstrate aberrant SPARC-dependent ECM remodeling in 3D**
4 **engineered fibrotic tissue of clinically relevant thickness**

6 **Authors**

7 Hiroyoshi Y. Tanaka^a, Kentaro Kitahara^a, Naoki Sasaki^{b,1}, Natsumi Nakao^a, Kae Sato^b, Hirokazu
8 Narita^c, Hiroshi Shimoda^c, Michiya Matsusaki^d, Hiroshi Nishihara^e, Atsushi Masamune^f, Mitsunobu
9 R. Kano^{a,g}

11 **Affiliations**

12 ^a Department of Pharmaceutical Biomedicine, Okayama University Graduate School of Medicine,
13 Dentistry, and Pharmaceutical Sciences, Okayama, Okayama, Japan.

14 ^b Department of Chemical and Biological Sciences, Japan Women's University, Bunkyo-Ku, Tokyo,
15 Japan.

16 ^c Department of Anatomical Science, Hirosaki University Graduate School of Medicine, Hirosaki,
17 Aomori, Japan.

18 ^d Department of Frontier Biosciences, Osaka University Graduate School of Frontier Biosciences,
19 Suita, Osaka, Japan.

20 ^e Genomics Unit, Keio Cancer Center, Keio University School of Medicine, Institute of Integrated
21 Medical Research, Shinjuku-ku, Tokyo, Japan.

22 ^f Division of Gastroenterology, Tohoku University Graduate School of Medicine, Sendai, Miyagi,
23 Japan.

24 ^g Department of Pharmaceutical Biomedicine, Okayama University Graduate School of
25 Interdisciplinary Science and Engineering in Health Systems, Okayama, Okayama, Japan.

26 ¹ Present address: Department of Applied Chemistry, Faculty of Science and Engineering, Toyo
27 University, Kawagoe, Saitama, Japan.

29 **Contact information**

30 Mitsunobu R. Kano, MD, PhD
31 Department of Pharmaceutical Biomedicine, Okayama University Graduate School of Medicine,
32 Dentistry, and Pharmaceutical Sciences

33 Department of Pharmaceutical Biomedicine, Okayama University Graduate School of
34 Interdisciplinary Science and Engineering in Health Systems
35 1-1-1 Tsushima-Naka, Kita-Ku, Okayama-shi, Okayama, 700-8530 Japan
36
37 E-mail: mikano-ky@umin.net

38 **Abbreviations**

39 3D: three-dimensional

40 CM: conditioned medium

41 DMSO: dimethyl sulfoxide

42 ECM: extracellular matrix

43 FN: Fibronectin

44 MMP: Matrix Metalloproteinase

45 PBS: phosphate-buffered saline

46 PSC: pancreatic stellate cells

47 ROCK: Rho-associated Kinase

48 RT: room temperature

49 RT-qPCR: reverse transcription quantitative polymerase chain reaction

50 S.D.: standard deviation

51 SPARC: Secreted Protein, Acidic and Rich in Cysteine

52 TGF- β : Transforming Growth Factor- β

53 **Abstract**

54 Desmoplasia is a hallmark of pancreatic cancer and consists of fibrotic cells and secreted extracellular
55 matrix (ECM) components. Various *in vitro* three-dimensional (3D) models of desmoplasia have been
56 reported, but little is known about the relevant thickness of the engineered fibrotic tissue. We thus
57 measured the thickness of fibrotic tissue in human pancreatic cancer, as defined by the distance from
58 the blood vessel wall to tumor cells. We then generated a 3D fibrosis model with a thickness reaching
59 the clinically observed range using pancreatic stellate cells (PSCs), the main cellular constituent of
60 pancreatic cancer desmoplasia. Using this model, we found that Collagen fiber deposition was
61 increased and Fibronectin fibril orientation drastically remodeled by PSCs, but not normal fibroblasts,
62 in a manner dependent on Transforming Growth Factor (TGF)- β /Rho-Associated Kinase (ROCK)
63 signaling and Matrix Metalloproteinase (MMP) activity. Finally, by targeting Secreted Protein, Acidic
64 and Rich in Cysteine (SPARC) by siRNA, we found that *SPARC* expression in PSCs was necessary
65 for ECM remodeling. Taken together, we developed a 3D fibrosis model of pancreatic cancer with a
66 clinically relevant thickness and observed aberrant SPARC-dependent ECM remodeling in cancer-
67 derived PSCs.

68

69 **Keywords**

70 Fibrosis; Extracellular Matrix Remodeling; 3D Culture; Pancreatic Stellate Cell; SPARC

71 **Impact Statement**

72 This paper describes a novel and facile *in vitro* model of pancreatic cancer desmoplasia with a
73 clinically relevant thickness that allows the study of extracellular matrix (ECM) remodeling. We
74 demonstrate that human pancreatic cancer derived pancreatic stellate cells (PSCs), the main
75 cellular constituent of the desmoplastic reaction, demonstrate pathological ECM remodeling via
76 a TGF- β /ROCK axis and MMP activity-dependent mechanism. We finally uncover a previously
77 unknown role of SPARC, a multifunctional glycoprotein associated with worse prognosis in
78 pancreatic cancer, in pathological Fibronectin fibril alignment by PSCs.

79 **1. Introduction**

80 Pancreatic adenocarcinoma is a recalcitrant malignancy with poor prognosis. It is
81 histopathologically characterized by desmoplasia, consisting of densely packed fibrotic stromal cells
82 and the extracellular matrix (ECM) components such as Collagen I and Fibronectin that these
83 stromal cells abundantly secrete [1]. The principal stromal cell type of desmoplasia in pancreatic
84 cancer is the pancreatic stellate cell (PSC) [2–6]. PSCs play a pivotal role in promoting the
85 desmoplastic reaction not only through production and secretion of ECM components but also
86 through active remodeling of the ECM [7,8]. Cancer-specific changes in ECM architecture have
87 gained great interest with increased recognition that aberrant ECM architecture has therapeutic
88 consequences through its effects on tumor solid mechanics [9], alteration of cancer cell
89 migration/invasion [7,8,10–12], and drug penetration into the tumor [13–16]. The desmoplastic
90 reaction is thus an important therapeutic target in pancreatic cancer, although recent papers highlight
91 potential pitfalls of simply ablating fibrotic cells [17–19] and point at the importance of
92 “reprogramming” them to a tumor-suppressive state [20,21]. There is thus an urgent need to model
93 and analyze fibrotic lesions within pancreatic cancer to elucidate the detailed mechanisms of
94 pathogenesis and identify therapeutic targets [22].

95 Recently, various three-dimensional (3D) culture techniques have been utilized to study
96 intratumoral fibrosis *in vitro* [23], with successful application in studying ECM architecture [24,25],
97 cancer cell migration [8,10,26,27], cancer-stroma crosstalk [8,28–30], and drug delivery [28,31,32].
98 Notably, it has recently been shown, albeit in a murine model of cardiac fibrosis and not intratumoral
99 fibrosis, that the topological arrangement of fibroblasts in 3D itself induces a fibrotic phenotype in
100 fibroblasts [33]. While this study seems to suggest that the thickness of fibrotic tissue itself may be a
101 self-sustaining driver of the fibrotic process, the spheroid model as used in this study generally
102 requires greatly different culture-ware and media for the generation of 3D spheroids compared to

103 conventional 2D culture. Furthermore, controlling spheroid size is usually technically challenging
104 [34]. Comparison of spheroids and conventional 2D culture cannot, therefore, be made
105 unequivocally with respect to tissue thickness. Our understanding of the importance of fibrotic tissue
106 thickness thus would greatly improve if a 3D model in which thickness can be easily experimentally
107 manipulated within a clinically relevant range is established. However, little is known quantitatively
108 about the clinically relevant thickness of engineered 3D models of fibrosis.

109 Thus, we in this study report 1) the clinically observed thickness of fibrotic lesions in human
110 pancreatic adenocarcinoma, 2) generation of 3D fibrotic tissues out of human pancreatic cancer-
111 derived PSCs recapitulating this thickness, 3) a demonstration of the potential of these 3D tissues to
112 study cancer-specific changes in ECM architecture. Furthermore, we study the role of Secreted
113 Protein, Acidic and Rich in Cysteine (SPARC), an important regulator of ECM assembly [35] also
114 implicated in PSC biology and associated with a worse prognosis in pancreatic cancer [36–39]. We
115 uncover a previously unknown role of SPARC in Fibronectin remodeling by PSCs.

116

117 **2. Materials & Methods**

118 **2.1. Histological analysis of fibrosis in human pancreatic adenocarcinoma**

119 For thickness measurements, images of tissue samples that we have previously stained and
120 characterized [40] were used. The histopathological evaluations and staging as demonstrated in
121 **Figure 1D and 1E** were made in this previous report. The thickness of fibrotic tissue was defined as
122 the distance from an intratumoral vessel wall to the most nearby tumor cell nest. Blood vessels in
123 areas of strong Platelet-Derived Growth Factor Receptor- β (PDGFR- β) positivity within the stroma
124 were selected from analysis due to the negative prognostic significance of stromal PDGFR- β
125 staining [40]. Furthermore, in light of the increasing use of 3D models to assess drug delivery, we
126 limited our analyses to precapillary arterioles to postcapillary venules since this is where drug

127 release from the bloodstream mainly occurs [41]. These blood vessels are typically characterized by
128 diameters of <50 μm or, approximately, a vessel perimeter of <150 μm . We thus excluded larger
129 vessels, defined as blood vessels with a wall perimeter >150 μm . 50 thickness measurements in total
130 were made per patient.

131

132 **2.2. Cell culture and reagents**

133 MRC5 and CAPAN-2 cells were obtained from American Type Cell Collection (Manassas, VA,
134 USA). Primary PSCs were obtained from human pancreatic adenocarcinoma patients as previously
135 described [42]. For PSC #1 and PSC #2 cell lines, immortalization was performed as previously
136 described [43]. MRC5, PSC #1, and PSC #2 cells were maintained in Dulbecco's Modified Eagle
137 medium (gibco/Thermo Fisher Scientific, Eugene, MA, USA) supplemented with 10% fetal bovine
138 serum, 50 U/mL penicillin, and 50 $\mu\text{g}/\text{mL}$ streptomycin. Primary PSCs were maintained in
139 Dulbecco's Modified Eagle medium/Ham's F-12 1:1 mixture (Sigma-Aldrich, St. Louis, MO, USA)
140 supplemented with 10% fetal bovine serum, 50 U/mL penicillin, and 50 $\mu\text{g}/\text{mL}$ streptomycin.
141 CAPAN-2 cells were maintained in McCoy's 5A medium (Sigma-Aldrich) supplemented with 10%
142 fetal bovine serum, 2 mM L-glutamine, 50 U/mL penicillin, and 50 $\mu\text{g}/\text{mL}$ streptomycin. To obtain
143 CAPAN-2 conditioned media (CM), CAPAN-2 cells grown to 80% confluence were then cultured in
144 Dulbecco's Modified Eagle Medium for another 24 hours. CM was then collected, passed through a
145 0.22 μm PVDF membrane filter (Merck Millipore, Burlington, MA, USA) to remove cell debris, and
146 stored frozen until use. For 3D tissue generation, trypsinized cells were first incubated in Tris-
147 buffered saline containing 150 mM sodium chloride, 0.04 mg/mL Fibronectin (Sigma-Aldrich), and
148 0.04 mg/mL Gelatin (Wako Pure Chemicals, Osaka, Japan) upon gentle rocking (30 min, RT). The
149 cells were then briefly centrifuged and re-suspended in their respective culture media before being
150 seeded on cell culture inserts for 24 well plates (0.4 μm , transparent; BD Falcon/Corning, Corning,

151 NY, USA) coated with 0.12 mg/mL Fibronectin. The cell culture reagents used in this study are as
152 follows: GM6001 (10 μ M in dimethyl sulfoxide [DMSO]; Calbiochem, San Diego, CA, USA),
153 LY364947 (10 μ M in DMSO; Calbiochem), Recombinant Human TGF- β 2 (1 ng/mL; PeproTech,
154 Rocky Hill, NJ, USA), Recombinant Human TGF- β 3 (1 ng/mL; R&D Systems, Inc., Minneapolis,
155 MN, USA), Y27632 (10 μ M in DMSO; Calbiochem). CAPAN-2 CM and TGF β 3 were applied 4
156 hours after cell seeding, and inhibitors after 24 hours. siRNAs (10 nM; Sigma Genosys, Tokyo,
157 Japan; sequences are shown in **Supplementary Table 1**) were transfected using Lipofectamine
158 RNAiMax (Invitrogen/Thermo Fisher Scientific). Cells were harvested for generating 3D tissues 24
159 hours after siRNA transfection.

160

161 **2.3. Thickness measurements of 3D tissues**

162 After two days of culture, 3D tissues were fixed with 4% (w/v) paraformaldehyde in phosphate
163 buffered saline (PBS; 5 min, RT), permeabilized with 0.2% (v/v) Triton X-100 in PBS (5 min, RT).
164 Nuclei were then stained with SYTOX Green nucleic acid stain (0.2 μ M, 30 min, RT; Molecular
165 Probes/Thermo Fisher Scientific). After washing with PBS thrice, culture insert membranes were
166 carefully excised using a scalpel and mounted on coverslips using fluorescent mounting medium
167 (Dako/Agilent, Santa Clara, CA, USA). Samples were then observed under a Nikon C2+ confocal
168 laser microscope (Tokyo, Japan), and Z-stack images of 0.2 μ m slices were obtained. Images were
169 3D-reconstituted and the thickness determined using the NIS-Elements AR version 4.30 software
170 (Nikon).

171

172 **2.4. Immunofluorescent staining and quantification**

173 After two or three days of culture with respective treatments, 3D tissues were fixed with 4%
174 (w/v) paraformaldehyde in PBS (5 min, RT), and blocked with Blocking One (nacalai tesque, Kyoto,

175 Japan; 1-2 hours, RT). 3D tissues were then incubated overnight at 4°C with primary antibodies
176 diluted in Blocking One. Primary antibodies used in this study are rabbit anti-Collagen I monoclonal
177 antibody (1/1000 dilution; clone EPR7785, ab138492, Abcam, Cambridge, UK), and rabbit anti-
178 Fibronectin polyclonal antibody (1/1000 dilution; F3468, Sigma). After washing with PBS thrice, 3D
179 tissues were incubated with Goat anti-Rabbit IgG (H+L) Cross-Adsorbed Secondary Antibody,
180 Alexa Fluor 594 (A-11012; Molecular Probes/Thermo Fisher Scientific) diluted in Blocking One
181 (1/200 dilution, 1-2 h, RT). After washing with PBS thrice, culture insert membranes were prepared
182 as above and observed under a Nikon C2+ confocal laser microscope. Fluorescence intensity of
183 Collagen I was quantified using ImageJ (NIH, Bethesda, MD, USA). For quantification of
184 Fibronectin orientation, acquired images were analyzed using Orientation J[44] plug-in on ImageJ.
185 To facilitate comparison between experimental groups, orientation graphs were prepared on
186 GraphPad Prism 6 (GraphPad Software, Inc., La Jolla, CA, USA) with the orientation angle showing
187 the maximum value set at 0 degrees. Based on this distribution curve, the orientation index was
188 defined as the area under the curve between -5 and 5 degrees divided by the area under the curve of
189 the whole distribution curve. The orientation index approaches 1 when all fibers are oriented
190 coherently within ± 5 degrees of each other, and $10/180=0.0555\dots$ when completely randomly
191 oriented.

192

193 **2.5. Reverse transcription quantitative polymerase chain reaction (RT-qPCR)**

194 Total RNA was isolated using TRI Reagent (Molecular Research Center, Cincinnati, OH, USA),
195 and reverse transcribed to complementary DNA (ReverTra Ace $-\alpha$ -; TOYOBO, Osaka, Japan)
196 according to the manufacturer's protocol. RT-qPCR was performed using THUNDERBIRD SYBR
197 qPCR mix (TOYOBO) using the StepOne Plus real-time PCR system (Applied Biosystems, Foster
198 City, CA, USA). Primers (Sigma Genosys) used are shown in **Supplementary Table 2**.

199

200 **2.6. Statistical analysis**

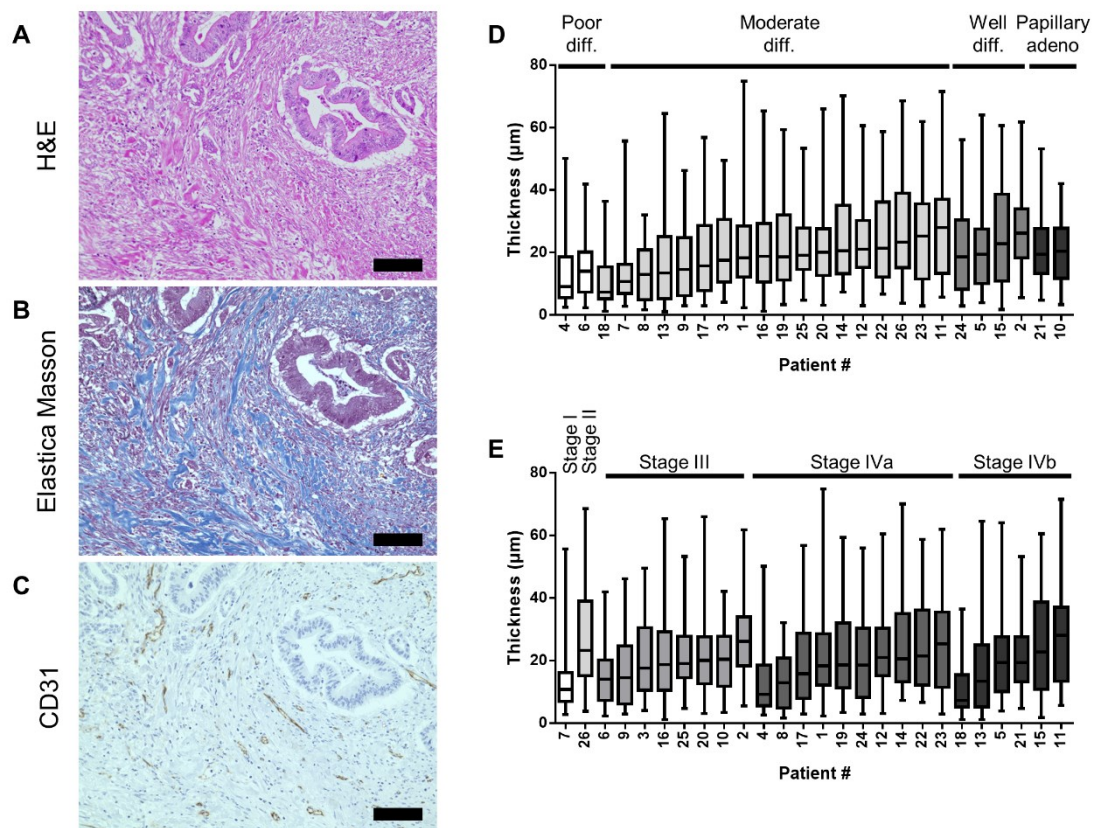
201 All data are presented as mean \pm S.D. For Collagen I quantification and RT-qPCR, data were
202 normalized with the mean of the reference condition set at 1. Statistical analyses were performed
203 using GraphPad Prism 6. For pooled data, sample sizes are indicated in the figure legend. For
204 experiments with two experimental groups, unpaired Student's *t*-test was performed. For
205 experiments with three or more experimental groups, one-way analysis of variance followed by *post*
206 *hoc* Dunnett's multiple comparisons test was performed unless otherwise noted. For data presented
207 in **Figure 7**, Tukey's multiple comparisons test was performed following two-way analysis of
208 variance. For all analyses, statistical significance was set at $p < 0.05$. In all figures: *n.s.*, *, **, ***,
209 and **** denote not significant, $p < 0.05$, $p < 0.01$, $p < 0.001$, $p < 0.0001$, respectively.

210

211 **3. Results**

212 **3.1. Median thickness of fibrotic tissue within human pancreatic cancer is between 10 to 30 μ m**

213 As shown in **Figure 1A-1C**, pancreatic cancer cells are embedded within thick fibrotic tissue at
214 a distance from blood vessels. We first characterized the "thickness" of fibrotic tissue, defined as the
215 distance from a blood vessel wall to the nearest nest of tumor cells (**Figure 1D and 1E**). This is the
216 least distance, we presumed, that an intravenously administered anti-tumor agent must pass through
217 to locate a tumor target. Analysis of fibrotic tissue thickness in 26 human pancreatic cancer
218 specimens revealed that there was a very large variation even within individual tumors, ranging from
219 a few micrometers up to 80 μ m. However, median thickness, regardless of the histological
220 differentiation status (**Figure 1D**) or clinical stage (**Figure 1E**), was generally between 10 to 30 μ m.



221

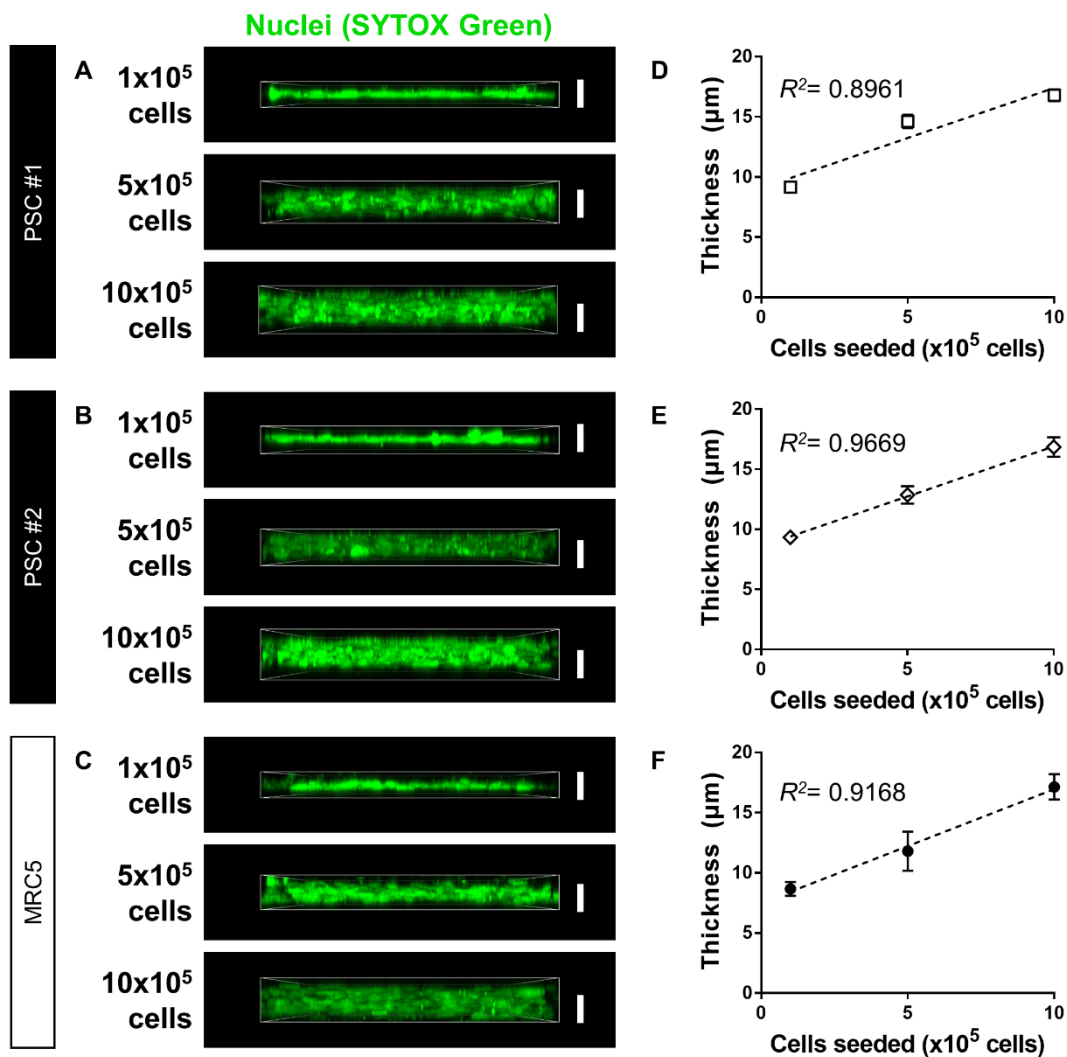
222 **Figure 1: Measurement of the thickness of fibrotic tissue in human pancreatic**
 223 **carcinoma specimens. (A-C)** Representative staining of serial sections obtained from
 224 human pancreatic adenocarcinoma by Hematoxylin and Eosin (H&E) (A), Elastica Masson
 225 (B), and for the endothelial marker CD31 (brown) (C). Scale bars = 100 μm. (D and E) For
 226 26 pancreatic adenocarcinoma patients of various histological differentiation status (D) and
 227 clinical stage (E), 50 measurements of thickness were made and shown in box-and-whisker
 228 plots (whiskers denote minimum to maximum, boxes denote interquartile range with a line
 229 drawn at the median).

230

231 3.2. Construction of 3D fibrotic tissues with a clinically relevant thickness

232 We first sought to create 3D fibrotic tissues within this range of thickness using PSCs or normal
 233 fibroblasts as a control. By seeding increasing numbers of the normal fibroblast cell line MRC5 or
 234 two immortalized PSC cell lines derived from different patients, we obtained 3D fibrotic tissues with
 235 thicknesses successfully surpassing 10 μm (Figure 2A-2C). Use of primary PSCs without

236 immortalization resulted in 3D tissues of greater thickness for the same number of cells seeded
 237 (Supplementary Figure 1A). Furthermore, the thickness of the obtained 3D fibrotic tissues
 238 generally correlated well linearly with the number of cells seeded (Figure 2D-2F, Supplementary
 239 Figure 1B).

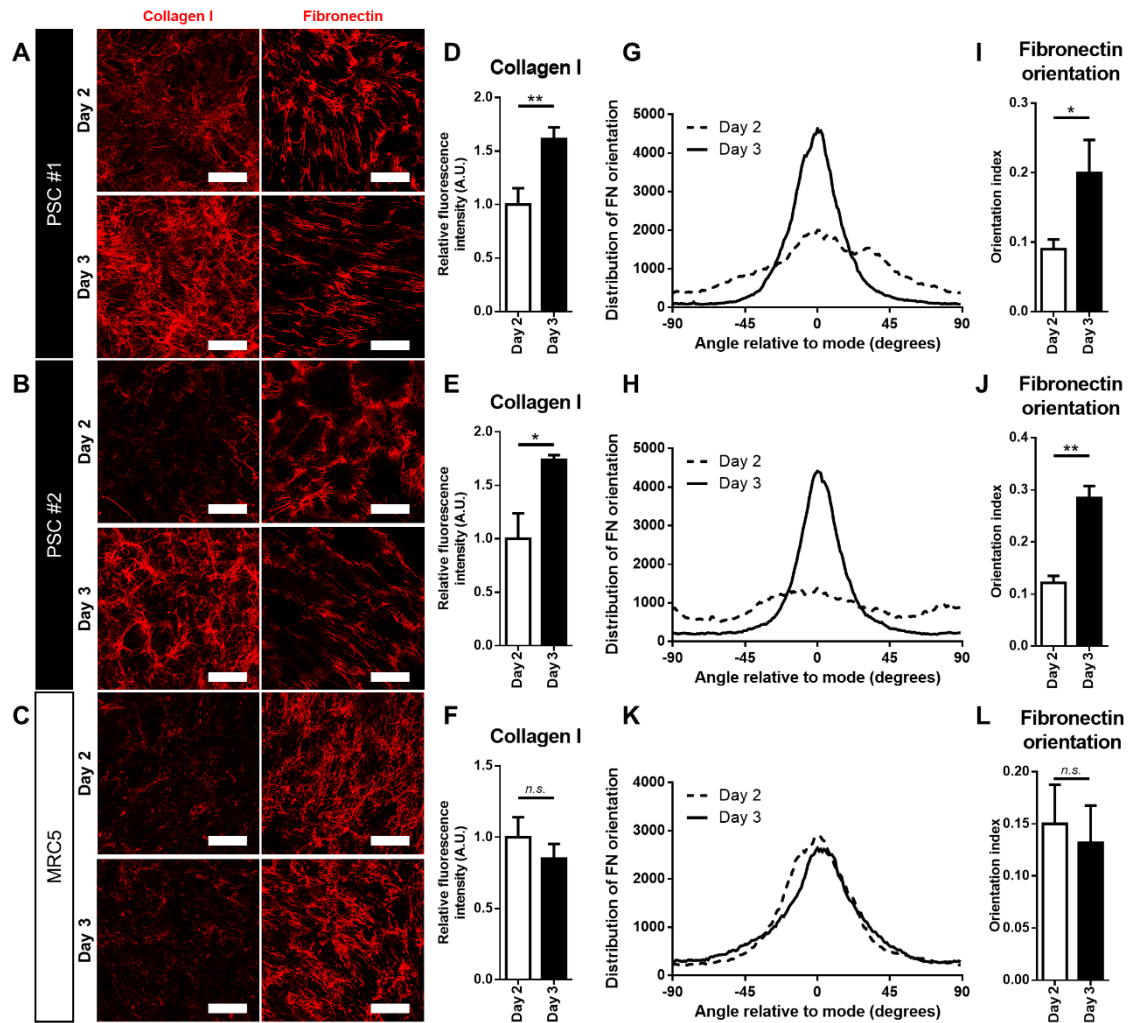


240
 241 **Figure 2: Recapitulation of the thickness of human pancreatic fibrotic tissue via 3-**
 242 **dimensional (3D) culture of pancreatic stellate cells (PSCs).** (A-C) Seeding of 1×, 5×, or
 243 10×10⁵ PSC #1 cells (A), PSC #2 cells (B), and control MRC5 fibroblasts cells (C) in 3D
 244 culture. Obtained 3D tissues were stained with SYTOX green (green), observed under a
 245 confocal laser microscope, and 3D-reconstituted. Representative vertical sectional images
 246 of the 3D tissues are shown. Scale bars = 10 μm. (D-F) Quantification of the thickness of the
 247 3D tissues obtained in (A), (B), and (C) ($n = 4$ for all experimental groups).

248

249 **3.3. PSCs demonstrate aberrant remodeling of Collagen I and Fibronectin**

250 ECM architecture is known to be altered in cancer with increased deposition of Collagen fibers
251 and coherence of Fibronectin fibril orientation [10–12,26], a change which in pancreatic cancer is
252 actively induced by PSCs [7,8]. Such aberrant ECM architecture in pancreatic cancer is generally
253 believed to affect therapeutic efficacy in various ways, such as through regulation of invasion and
254 effects on drug delivery [2,3,47,5,6,13,15,28,31,45,46]. We thus wondered whether our 3D fibrotic
255 tissue model recapitulates these cancer-specific ECM changes in Collagen deposition and
256 Fibronectin orientation. Indeed, we observed a dynamic change in ECM organization from day 2 to
257 day 3 of culture in PSCs but not control MRC5 fibroblasts. Collagen fibers were more clearly seen
258 on day 3 of culture in PSCs compared to day 2, whereas MRC5 fibroblasts demonstrated little
259 change during this period (**Figure 3A-3C**). Indeed, quantification of Collagen I fluorescence
260 revealed increased intensity on day 3 compared to day 2 in PSCs, but not MRC5 fibroblasts (**Figure**
261 **3D-3F**). Furthermore, the orientation of Fibronectin fibrils was more coherent in PSCs on day 3
262 compared to day 2 (**Figure 3G-J**), while MRC5 fibroblasts showed little change (**Figure 3K and**
263 **3L**). Use of primary PSCs without immortalization demonstrated consistent results (**Supplementary**
264 **Figure 2A-2D**). This was not necessarily accompanied by an increase in mRNA expression levels of
265 these ECM components within PSCs (**Supplementary Figure 3A-3D**), suggesting that PSCs indeed
266 actively remodel the ECM more than do MRC5 fibroblasts.



267

268

269

270

271

272

273

274

275

276

277

278

279

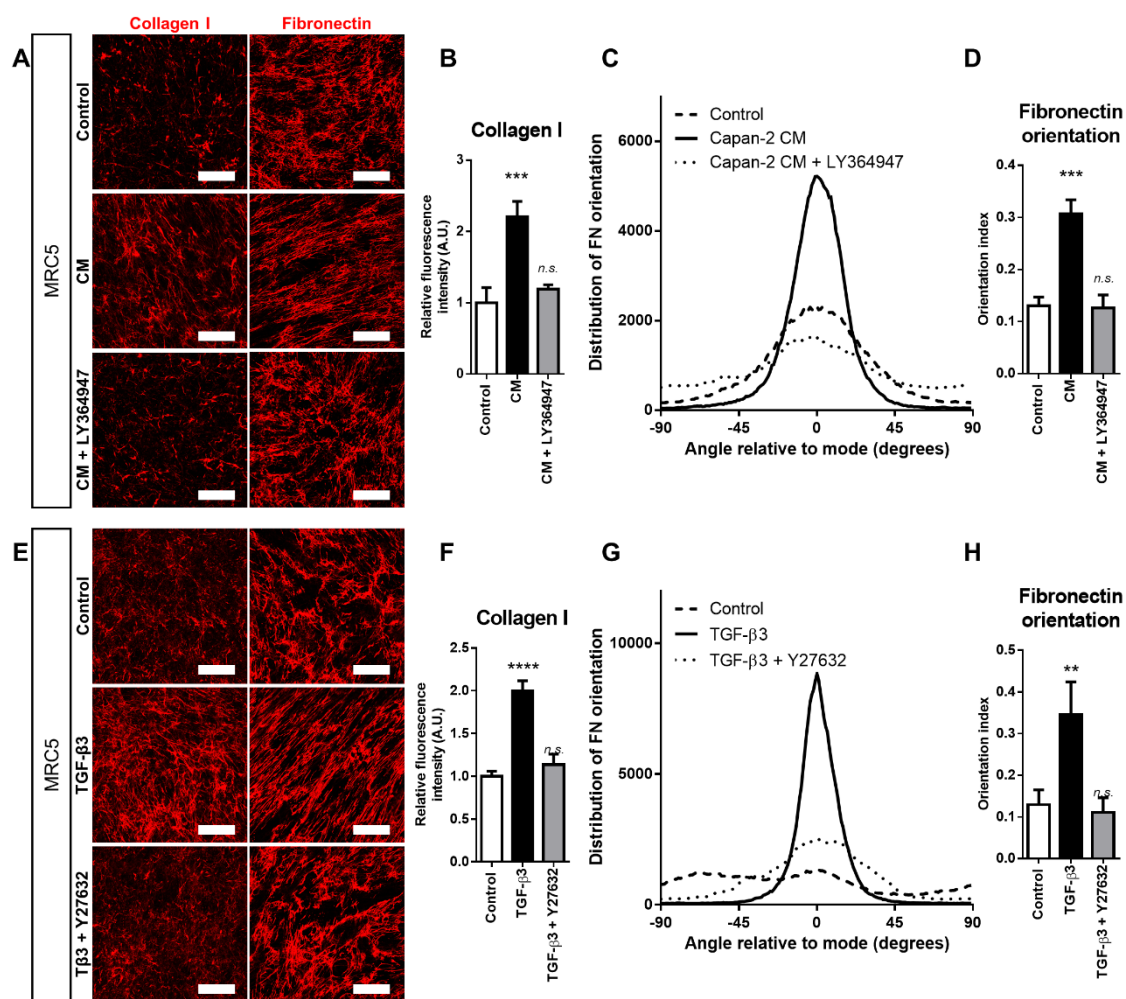
280

281

Figure 3: Extracellular matrix (ECM) remodeling in 3D tissue generated from PSCs but not normal fibroblasts. (A-C) Representative staining images of Collagen I (1st column, red) and Fibronectin (2nd column, red) in 3D tissues generated from seeding 5×10^5 PSC#1 cells (A), PSC #2 cells (B), or control MRC5 fibroblasts (C) after two or three days of culture. Scale bars = 50 μ m. (D-F) Quantification of the fluorescence intensity of Collagen I ($n = 3$ for all experimental groups) to compare between Day 2 (white bars) and Day 3 (black bars) of 3D culture. (G, H, and K) Representative curves demonstrating the distribution of FN orientation, corresponding to the images shown in the 2nd column of (A), (B), and (C) are shown. Broken lines depict distribution after two days of culture, solid lines after three days. (I, J, and L) Orientation index, the area under the curve between -5 and 5 degrees divided by the area under the curve for the whole orientation curves such as shown in (G), (H), and (K) to compare Day 2 (white bars) and Day 3 (black bars) of 3D culture ($n = 3$ for all experimental groups).

282 **3.4. Normal fibroblasts can be induced to demonstrate PSC-like ECM remodeling via a TGF-**
283 **β /ROCK axis-dependent mechanism**

284 We then sought to analyze the molecular mechanisms underlying this process. To this end, we
285 first wondered whether we could induce the normal MRC5 fibroblasts, which demonstrated a
286 minimal change in Collagen fiber amount and Fibronectin fibril orientation from day 2 to day 3, to a
287 “PSC-like” state by applying CM obtained from the pancreatic adenocarcinoma cell line, CAPAN-2.
288 Indeed, we found that 3D fibrotic tissue generated from MRC5 cells demonstrated increased
289 Collagen fiber deposition and coherence of Fibronectin fibril orientation when treated with CAPAN-
290 2 CM (**Figure 4A-4D**). Interestingly, treatment of MRC5 cells with the TGF- β inhibitor LY364947
291 annulled this CM-mediated induction of ECM remodeling (**Figure 4B and 4D**), suggesting that this
292 process was dependent on TGF- β signaling. Consistently, treating MRC5 fibroblasts with TGF- β 3
293 alone recapitulated the changes seen in Collagen fiber deposition and Fibronectin fibril alignment
294 with exposure to CAPAN-2 CM (**Figure 4E-4H**). Because ROCK, a downstream effector of TGF-
295 β [48], has previously been shown to be involved in Collagen I deposition in pancreatic cancer
296 stroma [49,50], we wondered whether ECM remodeling induced by TGF- β 3 in our model functions
297 through ROCK. Indeed, treatment with the ROCK inhibitor Y27632 reversed the changes induced
298 by TGF- β 3 not only in Collagen I deposition but also Fibronectin fibril orientation (**Figure 4F and**
299 **4H**).

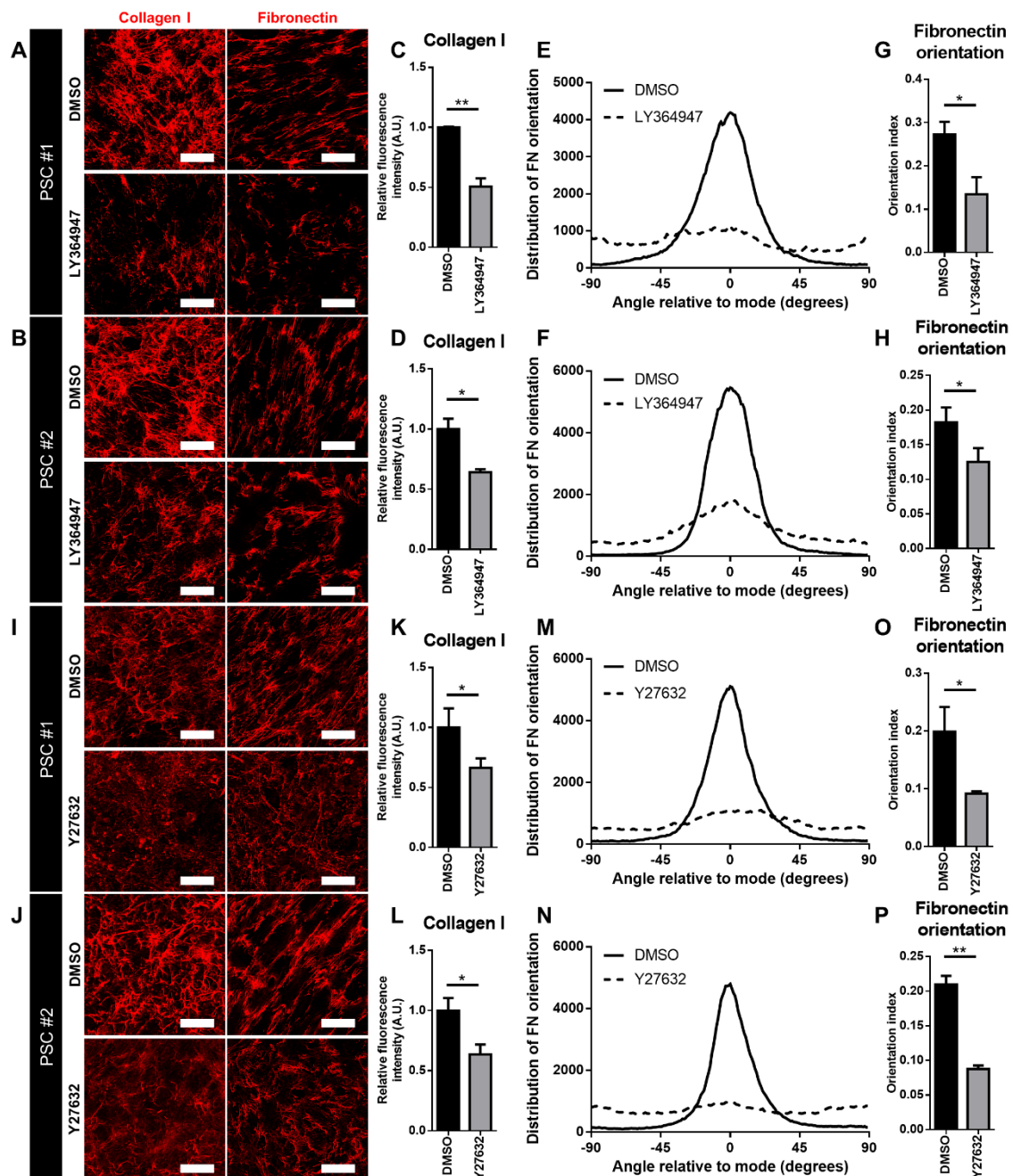


300
 301 **Figure 4: Transforming Growth Factor (TGF)-β signaling induced ECM remodeling in**
 302 **3D fibrotic tissue generated from normal fibroblasts via Rho-associated Kinase**
 303 **(ROCK). (A)** Representative staining images of Collagen I (1st column, red) and Fibronectin
 304 (2nd column, red) in 3D tissues generated from seeding 5×10^5 MRC5 fibroblasts cultured in
 305 unconditioned medium (first row), conditioned medium (CM) derived from the pancreatic
 306 ductal adenocarcinoma cell line CAPAN-2 (second row), or CAPAN-2 CM with the TGF-β
 307 receptor inhibitor LY364947 (third row). **(B)** Quantification of the fluorescence intensity of
 308 Collagen I ($n = 3$ for all experimental groups) to compare between control un-conditioned
 309 medium (white bar), CAPAN-2 CM (black bar), and CAPAN-2 CM in the presence of
 310 LY364947 (gray bar). **(C)** Representative curves demonstrating the distribution of FN
 311 orientation, corresponding to the images shown in the 2nd column of **(A)** are shown. Long
 312 dashed lines depict distribution for MRC5 cells cultured with unconditioned medium, solid
 313 lines with CAPAN-2 CM, and short dashed lines with CAPAN-2 CM in the presence of
 314 LY364947. **(D)** Orientation index was quantified from the orientation curves such as shown
 315 in **(C)** to compare between control un-conditioned medium (white bar), CAPAN-2 CM (black

316 bar), and CAPAN-2 CM in the presence of LY364947 (gray bar) ($n = 3$ for all experimental
317 groups). **(E)** Representative staining images of Collagen I (1st column, red) and Fibronectin
318 (2nd column, red) in 3D tissues generated from seeding 5×10^5 MRC5 fibroblasts cultured in
319 control medium (first row), with TGF- β 3 (second row), or with TGF- β 3 in the presence of
320 ROCK inhibitor Y27632 (third row). **(F)** Quantification of the fluorescence intensity of
321 Collagen I to compare between control (white bar), TGF- β 3 (black bar), and TGF- β 3 in the
322 presence of Y27632 (gray bar) ($n = 3$ for all experimental groups). **(G)** Representative curves
323 demonstrating the distribution of FN orientation, corresponding to the images shown in the
324 2nd column of **(E)** are shown. Long dashed lines depict distribution for MRC5 cells cultured
325 without TGF- β 3, solid lines with TGF- β 3, and short dashed lines with TGF- β 3 in the presence
326 of Y27632. **(H)** Orientation index was quantified from the orientation curves such as shown
327 in **(G)** to compare between control (white bar), TGF- β 3 (black bar), and TGF- β 3 in the
328 presence of Y27632 (gray bar) ($n = 3$ for all experimental groups). Scale bars = 50 μ m.
329

330 **3.5. Aberrant ECM remodeling by PSCs is dependent on TGF- β /ROCK axis**

331 Next, we investigated the involvement of TGF- β and its downstream effector ROCK in the
332 remodeling of ECM seen in 3D fibrotic tissues generated from PSCs. Consistent with the results
333 obtained from MRC5 cells, treatment of 3D PSC fibrotic tissues with LY364947 (**Figure 5A-5H**) or
334 Y27632 (**Figure 5I-5P**) reduced the deposition of Collagen fibers (**Figure 5C, 5D, 5G, and 5H**) and
335 largely randomized Fibronectin fibril orientation (**Figure 5K, 5L, 5O, and 5P**) on day 3 of culture.



336

337

338

339

340

341

342

343

344

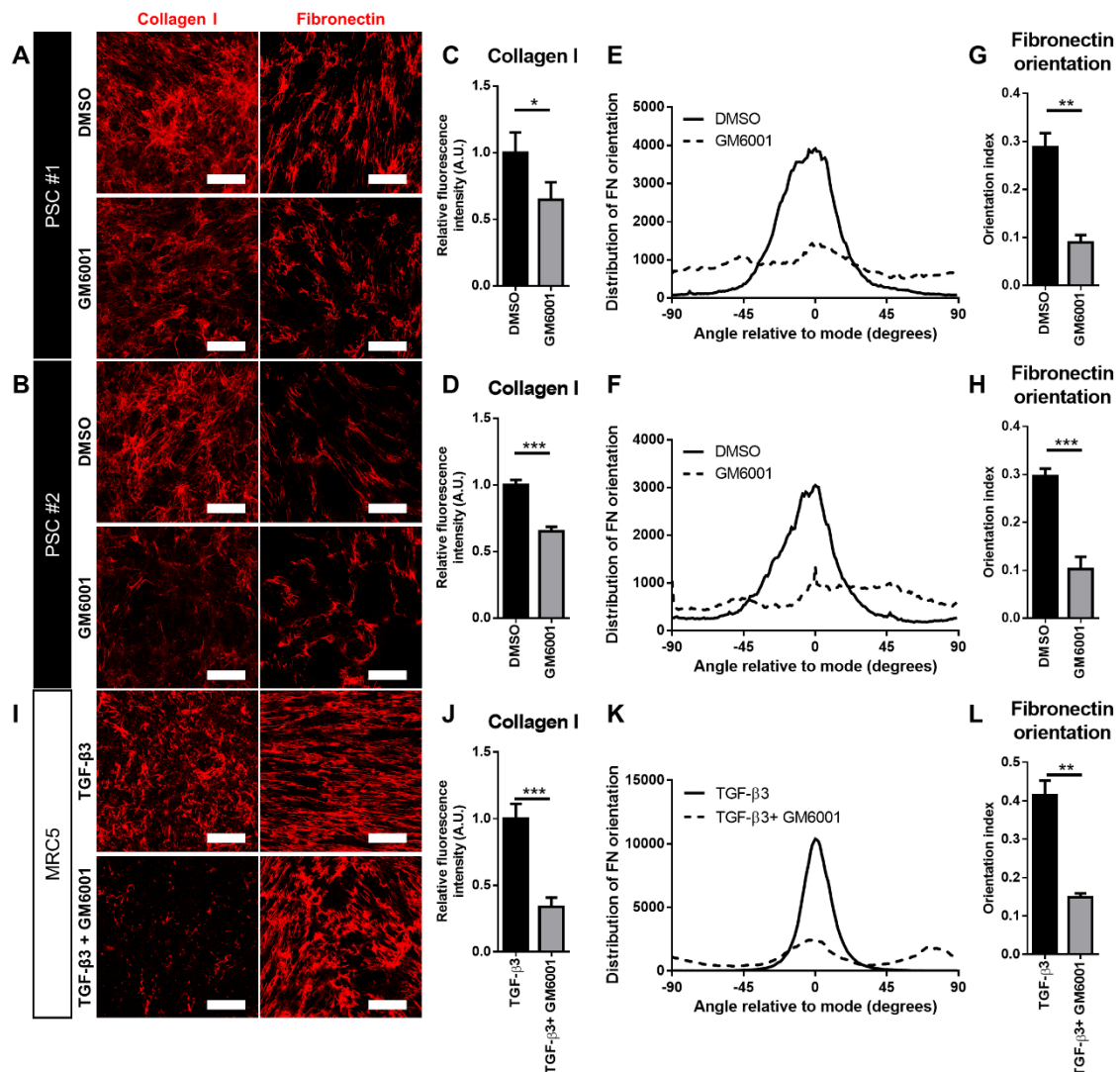
Figure 5: Inhibition of TGF- β or ROCK abrogated ECM remodeling seen in 3D fibrotic tissue generated from PSCs. (A and B) Representative staining images of Collagen I (1st column, red) and Fibronectin (2nd column, red) in 3D tissues generated from seeding 5×10^5 PSC #1 cells (A) or PSC #2 cells (B) without (top row) or in the presence of LY364947 (bottom row). (C and D) Quantification of the fluorescence intensity of Collagen I ($n = 3$ for all experimental groups) to compare between DMSO control (black bars) and LY364947 (gray bars). (E and F) Representative curves demonstrating the distribution of FN orientation, corresponding to the images shown in the 2nd column of (A) and (B) are shown. Solid lines

345 depict distribution without LY364947, and broken lines with. (**G and H**) Orientation index was
346 quantified from the orientation curves such as shown in (**E**) and (**F**) to compare between
347 DMSO control (black bars) and LY364947 (gray bars) ($n = 3$ for all experimental groups). (**I**
348 **and J**) Representative staining images of Collagen I (1st column, red) and Fibronectin (2nd
349 column, red) in 3D tissues generated from seeding 5×10^5 PSC #1 cells (**C**) or PSC #2 cells
350 (**D**) without (top row) or in the presence of Y27632 (bottom row). (**K and L**) Quantification of
351 the fluorescence intensity of Collagen I to compare between DMSO control (black bars) and
352 Y27632 (gray bars) ($n = 3$ for all experimental groups). (**M and N**) Representative curves
353 demonstrating the distribution of FN orientation, corresponding to the images shown in the
354 2nd column of (**I**) and (**J**) are shown. Solid lines depict distribution without Y27632, and broken
355 lines with. (**O and P**) Orientation index was quantified from the orientation curves such as
356 shown in (**M**) and (**N**) to compare between DMSO control (black bars) and Y27632 (gray
357 bars) ($n = 3$ for all experimental groups). Scale bars = 50 μm .

358

359 **3.6. Aberrant ECM remodeling by PSCs is dependent on MMP activity**

360 Because MMPs are well-known players in ECM remodeling within the tumor microenvironment
361 [51], expressed by PSCs downstream of TGF- β [52,53], and furthermore regulated downstream of
362 Rho/ROCK [54–57], we assessed whether MMPs are involved in the ECM remodeling observed in
363 our 3D fibrotic tissue model. Broad inhibition of MMP activity using the inhibitor GM6001
364 attenuated the increase of Collagen fiber amount and coherence of Fibronectin fibril orientation in
365 PSCs (**Figure 6A-6H**) and MRC5 fibroblasts activated with TGF- β 3 (**Figure 6I-6L**). This suggests
366 that MMP activity is requisite for the ECM remodeling observed in our 3D fibrosis model of
367 pancreatic cancer.



368

369

370

371

372

373

374

375

376

377

378

379

380

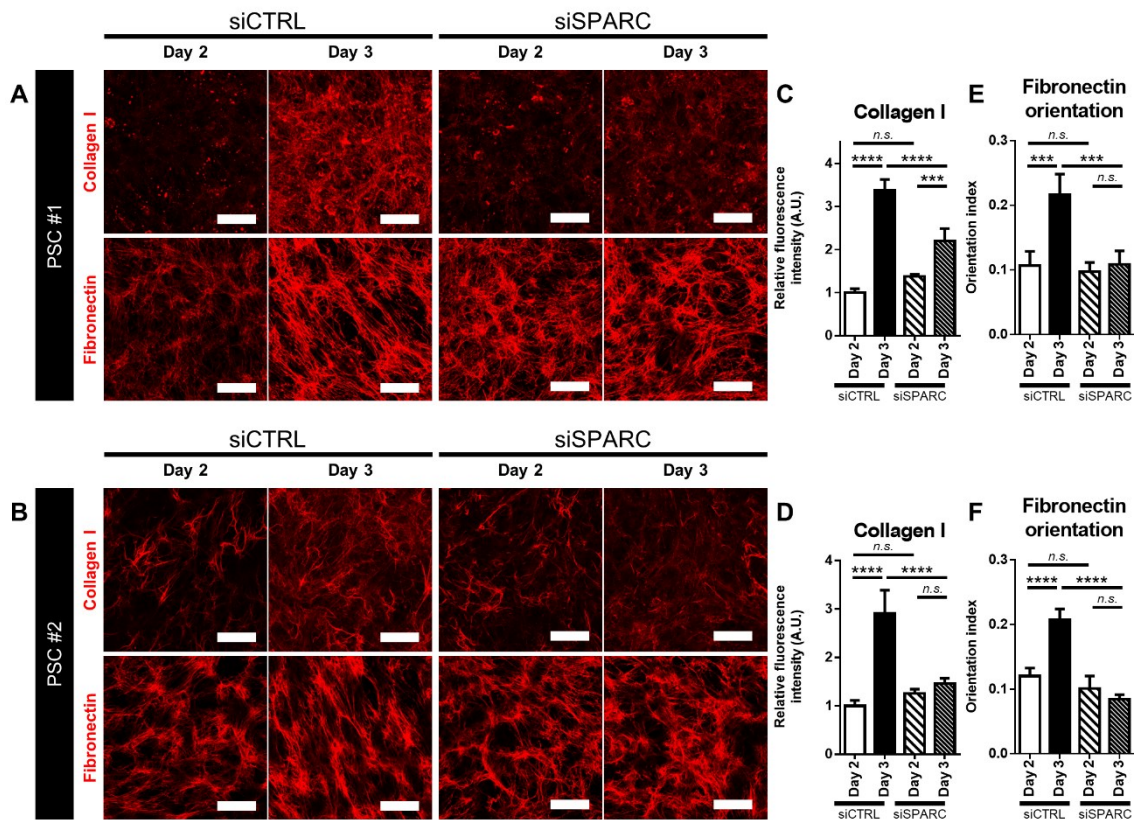
381

Figure 6: Matrix Metalloprotease (MMP) activity was indispensable for ECM remodeling seen in 3D fibrotic tissue. (A and B) Representative staining images of Collagen I (1st column, red) and Fibronectin (2nd column, red) in 3D tissues generated from seeding 5×10^5 PSC #1 cells (A) or PSC #2 cells (B) without (top row) or in the presence of the MMP inhibitor GM6001 (bottom row). (C and D) Quantification of the fluorescence intensity of Collagen I to compare between DMSO control (black bars) and GM6001 (gray bars) ($n = 4$ for PSC #1 cells, $n = 3$ for PSC #2 cells). (E and F) Representative curves demonstrating the distribution of FN orientation, corresponding to the images shown in the 2nd column of (A) and (B) are shown. Solid lines depict distribution without GM6001, and broken lines with. (G and H) Orientation index was quantified from the orientation curves such as shown in (E) and (F) to compare between DMSO control (black bars) and GM6001 (gray bars) ($n = 3$ for all experimental groups). (I) Representative staining images of Collagen I (1st column, red) and Fibronectin (2nd column, red) in 3D tissues generated from seeding

382 5×10^5 MRC5 cells with TGF- β alone (top row) or together with GM6001 (bottom row). **(J)**
383 Quantification of the fluorescence intensity of Collagen I to compare between TGF- β 3 (black
384 bar) and TGF- β 3 in the presence of GM6001 (gray bar) ($n = 4$ for both experimental groups).
385 **(K)** Representative curves demonstrating the distribution of FN orientation, corresponding to
386 the images shown in the 2nd column of **(I)** are shown. Solid lines depict distribution without
387 GM6001, and broken lines with. **(L)** Orientation index was quantified from the orientation
388 curves such as shown in **(K)** to compare between TGF- β 3 (black bar) and TGF- β 3 in the
389 presence of GM6001 (gray bar) ($n = 3$ for both experimental groups). Scale bars = 50 μ m.
390

391 **3.7. Aberrant ECM remodeling by PSCs is dependent on SPARC**

392 We then sought to utilize our 3D fibrotic tissue model to assess whether SPARC, a multi-
393 functional glycoprotein which is an important player in ECM homeostasis [35] and the pathogenesis
394 of pancreatic cancer [36,37], is involved in the observed ECM remodeling process. We compared
395 Collagen fiber deposition and Fibronectin fibril orientation of 3D fibrotic tissue generated from
396 PSCs treated with either control siRNA or siRNA targeting *SPARC* (**Supplementary Figure 4A and**
397 **4B**). Though 3D tissues made of PSCs treated with control siRNA demonstrated increased Collagen
398 fiber deposition and coherence of Fibronectin fibril orientation, knockdown of *SPARC* in PSCs
399 largely blunted or completely abolished these changes (**Figure 7A-7F**). These results suggest that the
400 ECM remodeling demonstrated by PSCs is dependent on *SPARC* expression.



401

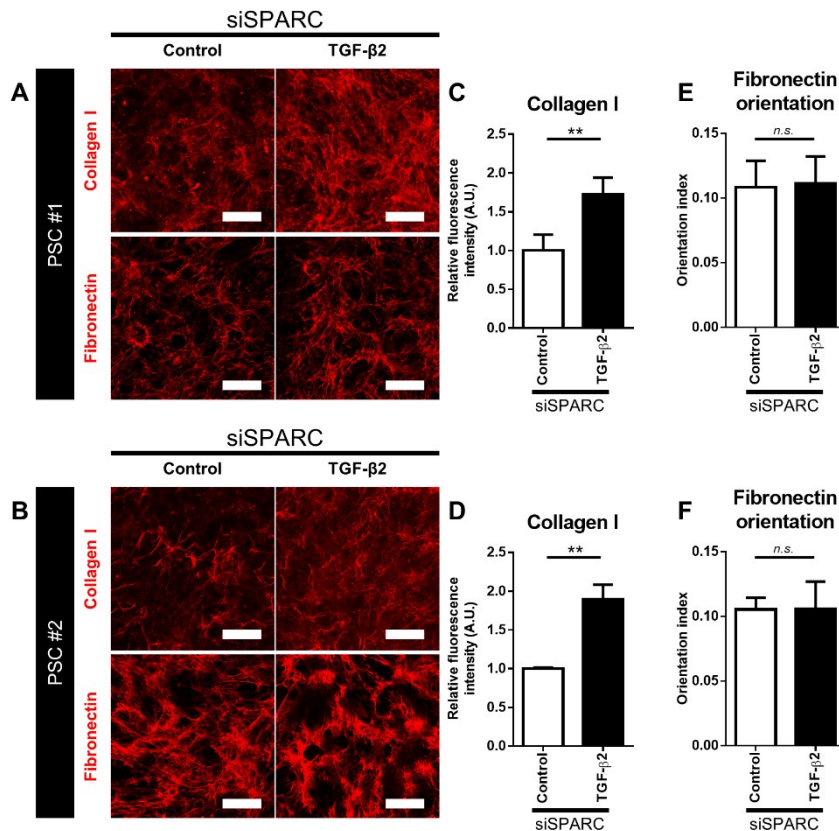
402 **Figure 7: SPARC expression was indispensable for ECM remodeling seen in 3D fibrotic**
 403 **tissue generated from PSCs. (A and B)** Representative staining images of Collagen I (1st
 404 row, red) and Fibronectin (2nd row, red) in 3D tissues generated from seeding 5×10^5 PSC #1
 405 cells (A) or PSC #2 cells (B) treated with control siRNA (siCTRL, first and second columns)
 406 or an siRNA against SPARC (siSPARC, third and fourth columns). The first and third columns
 407 are samples harvested on day 2, and the second and fourth columns on day 3 of 3D culture.
 408 (C and D) Quantification of the fluorescence intensity of Collagen I ($n = 4$ for each
 409 experimental group). (E and F) Orientation index of Fibronectin fibrils ($n = 4$ for each
 410 experimental group). In (C-F), light bars denote samples harvested on day 2, while the dark
 411 bars denote samples harvested on day 3. Simple bars denote samples treated with siCTRL
 412 and hashed bars with siSPARC. Scale bars = 50 μm .

413

414 3.8. SPARC regulates Collagen I and Fibronectin remodeling by distinct mechanisms

415 Finally, because *Sparc* knockout in murine mesangial cells has previously been reported to result
 416 in decreased TGF- β ligand and Collagen expression [58], we wondered whether the failure of PSCs
 417 to remodel the ECM after *SPARC* knockdown was due to altered TGF- β signaling and defective

418 ECM expression. We first quantified *COL1A1* and *FNI* mRNA expression observed no significant
419 changes (**Supplementary Figure 4C-4F**). Furthermore, of the three TGF- β isoforms, we found that
420 the mRNA expression level of *TGFB2* was significantly decreased upon *SPARC* knockdown in
421 PSCs, while the expression of *TGFB1* and *TGFB3* were unchanged (**Supplementary Figure 4G-**
422 **4L**). We then surmised that if decreased production of TGF- β ligand was the cause of the failure to
423 remodel the ECM, supplementation of TGF- β 2 ligand to PSCs treated with siRNA against *SPARC*
424 would rescue the remodeling defect seen upon *SPARC* knockdown. Indeed, administration of TGF-
425 β 2 ligand to PSCs induced an increase in Collagen I amount despite *SPARC* knockdown (**Figure 8A-**
426 **8D**). Interestingly, however, TGF- β 2 could not rescue the inability of PSCs to coherently align
427 Fibronectin fibrils upon *SPARC* knockdown (**Figure 8A, 8B, 8E, and 8F**). In line with these
428 findings, *SPARC* knockdown in MRC5 cells treated with TGF- β 2 could not inhibit the increase in
429 Collagen I amount (**Supplementary Figure 5A and 5B**), but did abrogate the alignment of
430 Fibronectin fibrils induced by TGF- β 2 (**Supplementary Figure 5A and 5C**). These results
431 altogether suggest that *SPARC* is necessary for ECM remodeling by PSCs, but regulates Collagen I
432 fiber deposition and alignment of Fibronectin fibril orientation via different mechanisms: the former
433 can at least partly be substituted by TGF- β 2 administration, but not the latter.



434

435

436

437

438

439

440

441

442

443

444

445

4. Discussion

446

447

448

449

The use of 3D culture methods in modeling disease states such as fibrosis has gained much interest recently [59,60]. We have adopted the distance from the blood vessel wall to the most nearby tumor nest as the definition of “thickness” in light of the use of these engineered fibrotic tissues as an *in vitro* model to assess drug delivery [23,28,31,32]. This is the length an intravenously

450 administered therapeutic agent must travel to locate a tumor target and exert its cytotoxic effects. We
451 found that a median thickness of 10 to 30 μm is seen across tumors from 26 patients, a range
452 comparable to a previous report for 8 patients [16]. By including patients of various histological
453 differentiation status or clinical stage, we furthermore assessed whether these factors may affect the
454 thickness of fibrotic tissue. However, the median thickness demonstrated no clear trend (**Figure 1**).

455 We then used immortalized human PSCs, or a normal fibroblast cell-line as control, to fabricate
456 3D fibrotic tissue models with this thickness (**Figure 2**). Use of non-immortalized primary PSCs
457 resulted in 3D tissues of greater thickness for the same number of cells seeded, presumably due to
458 the larger cell size compared to their immortalized counterpart. This facilitated the generation of 3D
459 tissues surpassing 20 μm (**Supplementary Figure 1**). We however mainly used immortalized human
460 PSCs for the mechanistic analyses in this study because a comparable thickness was obtained for the
461 same number of PSCs seeded compared to normal fibroblasts. While we in this study observed
462 similar remodeling of ECM in both primary and immortalized PSCs, immortalization is known in
463 certain cases to alter cellular phenotype. It thus seems necessary in future studies aimed at
464 elucidating the effect of thickness on the fibrotic phenotype of PSCs to be done or be confirmed also
465 using primary PSCs.

466 Using these 3D fibrotic tissues with a clinically relevant thickness, we then characterized and
467 compared the architecture of two major ECM components, Collagen I and Fibronectin, between
468 PSCs and normal fibroblasts (**Figure 3**). We found that PSCs demonstrate an increase in Collagen I
469 fiber content and coherence of Fibronectin fibril orientation between days 2 and 3 of culture, while
470 normal fibroblasts do not. This largely confirms previous studies reporting aberrant ECM
471 remodeling by cancer-associated fibroblasts [10,11,24]. Though we could discern the conspicuous
472 differences between PSCs and normal fibroblasts already on day 3 of culture, future studies aimed at
473 observing the remodeling of ECM structure over longer time-periods may yield additional

474 information. For Collagen I, such observation may be facilitated by the use of second harmonic
475 generation microscopy, a non-linear optical technique which enables Collagen fiber visualization
476 without staining even in live tissue [61–63]: an approach which warrants future investigation. Such
477 an approach, together with transmission electron microscopy experiments to analyze both the density
478 and ultrafine structure of the ECM, may yield an integrated understanding of pathological ECM
479 remodeling.

480 Furthermore, we showed that normal fibroblasts could be induced to demonstrate aberrant ECM
481 remodeling via treatment with CM derived from a pancreatic cancer cell line in a TGF- β signaling-
482 dependent manner, and furthermore simply by the administration of TGF- β via a ROCK and MMP-
483 dependent mechanism (**Figure 4 and 6**). Consistently, ECM remodeling demonstrated by PSCs was
484 also found to be dependent on TGF- β , ROCK, and MMP activity (**Figure 5 and 6**). The involvement
485 of TGF- β was predictable especially given its paramount importance in the pathogenesis of fibrotic
486 disorders [64]. Our findings add to gradually accumulating evidence that ROCK is an important
487 mediator in PSCs [49,50], and also perhaps cancer-associated fibroblasts in general [65–67].
488 Because MMPs constitute a large family [51], further detailed studies assessing the expression
489 profile of various MMPs in PSCs and the relative importance of each in ECM remodeling are
490 warranted. In future studies, we intend to utilize this 3D fibrosis model to study other ECM
491 components in addition to Collagen I and Fibronectin studied here.

492 We also used the 3D fibrotic tissue model to study the role of SPARC, a glycoprotein with a
493 myriad of reported functions and expressed by PSCs in pancreatic cancer [68]. Though there are now
494 conflicting reports [69,70], it had initially been suggested to affect the therapeutic efficacy of
495 pancreatic cancer patients treated with nab-paclitaxel [71]. It has also been demonstrated that
496 SPARC expression in peritumoral stroma portends a poor prognosis [38] and that it is highly
497 expressed in a subgroup of pancreatic patients who demonstrate an unfavorable “activated” stromal

498 gene signature [39]. The role of SPARC in ECM assembly was first suggested by the dermal
499 phenotype of *Sparc*-null mice which demonstrate decreased Collagen fiber diameter [72]. Since
500 then, numerous mechanisms by which SPARC affects and regulates ECM homeostasis have been
501 reported [35]. However, this is to the best of our knowledge the first report to address the role of
502 SPARC in Collagen I fiber deposition by PSCs. We have also uncovered a novel role of SPARC in
503 mediating the remodeling of Fibronectin fibers (**Figure 7**). Notably, though SPARC was
504 indispensable for both Collagen I fiber deposition and alignment of Fibronectin fibrils, the
505 mechanism by which SPARC regulates each remodeling process was different: TGF- β 2, the only
506 TGF- β isoform specifically down-regulated by *SPARC* knockdown, could rescue *SPARC* knockdown
507 for Collagen I fiber deposition but not alignment of Fibronectin fibrils (**Figure 8**), which suggests a
508 complex regulation of ECM remodeling by SPARC utilizing multiple pathways. The significance of
509 isoform-specific regulation of TGF- β and the distinct pathways by which Collagen I deposition and
510 Fibronectin alignment are regulated are both interesting questions we are currently investigating.

511 The 3D culture method used in the present study allowed the visualization of changes in ECM
512 structure as early as between days 2 and 3 of culture, compared to 6 to 10 days necessary for a
513 previously reported, well-characterized method [25]. The shorter experimental duration may
514 expedite mechanistic analyses or the screening for potential ECM-targeting drugs that normalize the
515 abnormal ECM remodeling process in pancreatic cancer. Our 3D fibrotic model may be used as an
516 alternative technique for *in vitro* analyses of tumor stroma in addition to previously established 3D
517 organotypic models embedding PSCs within ECM gels [73–75], or 3D spheroidal models
518 [8,32,76,77]. The advantage of our model is that it does not require different culture conditions to
519 generate tissues of different thickness; the number of cells seeded is the only factor which needs to
520 be tuned. However, whether the ECM structure observed in our 3D fibrosis model is amenable to
521 decellularization for use as ECM scaffolds in migration studies [10–12,26] warrants future

522 investigation. Furthermore, we have not assessed matrix density or stiffness. Additional steps such as
523 the administration of ascorbic acid [78] or prolongation of culture period to promote ECM
524 crosslinking and maturation may be required to attain the clinically observed range.

525

526 **5. Conclusions**

527 Altogether in this study, we report the clinically observed thickness of fibrotic lesions in human
528 pancreatic adenocarcinoma and achieve a thickness within this range with 3D fibrotic tissues
529 comprised of human PSCs. In addition, we present data demonstrating the promise of using these 3D
530 fibrotic tissue models in studying the mechanisms leading to pancreatic cancer-derived PSC-specific
531 alterations in ECM architecture, elucidating a previously unreported role of SPARC in ECM
532 remodeling by PSCs. Analysis of 3D fibrotic models together with the co-culture or incorporation of
533 pancreatic cancer cells, especially of differing mutational status [45], is a promising line of
534 investigation for the future and may be useful in modeling tumor-stroma interaction and its
535 consequences on ECM structure.

536

537 **Author Contributions**

538 HYT, KS, HS, MM, HNi, AM, and MRK participated in experimental design. HYT, KK, NS, NN,
539 and HNa conducted the experiments and data analyses. HYT and MRK wrote the manuscript which
540 was reviewed, edited, and approved by all co-authors.

541

542 **Conflicts of interest**

543 The authors have no conflicts of interest to disclose.

544

545 **Acknowledgments**

546 The authors deeply thank Dr. Hiromi Matsubara and Dr. Aiko Ogawa (National Hospital
547 Organization Okayama Medical Center) for the generous provision of experimental facilities, Dr.
548 Kazuki Nagashima (Stanford University) for valuable discussion and assistance, and Michael W.
549 Miller for editorial work. The authors are furthermore grateful to the members of the lab, especially
550 Taiki Oosato, Yuuki Kurahashi, Chiharu Morii, Yoshiko Okita, Kengo Harada, and Haruko Ohta for
551 insightful discussion and valuable technical assistance. This study was supported in part by Grant-in-
552 Aid for Scientific Research (KAKENHI) (26293119, 15H04804, 18H02797), Okayama University,
553 Kato Memorial Bioscience Foundation, the Mitsui Life Social Welfare Foundation, the Smoking
554 Research Foundation, the Pancreas Research Foundation of Japan, and JSPS Core-to-Core Program,
555 A. Advanced Research Networks. H.Y.T. was supported by a Ph.D. scholarship from the Takeda
556 Science Foundation.

557

558 **Data Availability**

559 The authors declare that all data supporting the findings of this study are available within the paper
560 and its Supplementary Information. Source data for the figures in this study are available from the
561 authors upon request.

562

563 **References**

- 564 [1] M. Schober, R. Jesenofsky, R. Faissner, C. Weidenauer, W. Hagmann, P. Michl, R. Heuchel, S.
565 Haas, J.-M. Löhr, Desmoplasia and Chemoresistance in Pancreatic Cancer, *Cancers (Basel)*. 6
566 (2014) 2137–2154. doi:10.3390/cancers6042137.
- 567 [2] M. V Apte, J.S. Wilson, A. Lugea, S.J. Pandol, A Starring Role for Stellate Cells in the Pancreatic

568 Cancer Microenvironment, *Gastroenterology*. 144 (2013) 1210–1219.
569 doi:10.1053/j.gastro.2012.11.037.

570 [3] M. Erkan, G. Adler, M. V Apte, M.G. Bachem, M. Buchholz, S. Detlefsen, I. Esposito, H. Friess,
571 T.M. Gress, H.-J. Habisch, R.F. Hwang, R. Jaster, J. Kleeff, G. Klöppel, C. Kordes, C.D.
572 Logsdon, A. Masamune, C.W. Michalski, J. Oh, P.A. Phillips, M. Pinzani, C. Reiser-Erkan, H.
573 Tsukamoto, J. Wilson, StellaTUM: current consensus and discussion on pancreatic stellate cell
574 research, *Gut*. 61 (2012) 172–178. doi:10.1136/gutjnl-2011-301220.

575 [4] D. Mahadevan, D.D. Von Hoff, Tumor-stroma interactions in pancreatic ductal adenocarcinoma,
576 *Mol. Cancer Ther.* 6 (2007) 1186–1197. doi:10.1158/1535-7163.MCT-06-0686.

577 [5] M. Erkan, S. Hausmann, C.W. Michalski, A.A. Fingerle, M. Dobritz, J. Kleeff, H. Friess, The
578 role of stroma in pancreatic cancer: diagnostic and therapeutic implications, *Nat. Rev.*
579 *Gastroenterol. Hepatol.* 9 (2012) 454–467. doi:10.1038/nrgastro.2012.115.

580 [6] A. Masamune, T. Watanabe, K. Kikuta, T. Shimosegawa, Roles of Pancreatic Stellate Cells in
581 Pancreatic Inflammation and Fibrosis, *Clin. Gastroenterol. Hepatol.* 7 (2009) S48–S54.
582 doi:10.1016/j.cgh.2009.07.038.

583 [7] K. Koikawa, K. Ohuchida, S. Takesue, Y. Ando, S. Kibe, H. Nakayama, S. Endo, T. Abe, T.
584 Okumura, K. Horioka, M. Sada, C. Iwamoto, T. Moriyama, K. Nakata, Y. Miyasaka, R.
585 Ohuchida, T. Manabe, T. Ohtsuka, E. Nagai, K. Mizumoto, M. Hashizume, M. Nakamura,
586 Pancreatic stellate cells reorganize matrix components and lead pancreatic cancer invasion via the
587 function of Endo180, *Cancer Lett.* (2017). doi:10.1016/j.canlet.2017.10.010.

588 [8] C.R. Drifka, A.G. Loeffler, C.R. Esquibel, S.M. Weber, K.W. Eliceiri, W.J. Kao, Human
589 pancreatic stellate cells modulate 3D collagen alignment to promote the migration of pancreatic
590 ductal adenocarcinoma cells, *Biomed. Microdevices.* 18 (2016) 105. doi:10.1007/s10544-016-
591 0128-1.

- 592 [9] T. Stylianopoulos, The Solid Mechanics of Cancer and Strategies for Improved Therapy, J.
593 Biomech. Eng. 139 (2017) 021004. doi:10.1115/1.4034991.
- 594 [10] J.G. Goetz, S. Minguet, I. Navarro-Lérida, J.J. Lazcano, R. Samaniego, E. Calvo, M. Tello, T.
595 Osteso-Ibáñez, T. Pellinen, A. Echarri, A. Cerezo, A.J.P. Klein-Szanto, R. Garcia, P.J. Keely, P.
596 Sánchez-Mateos, E. Cukierman, M.A. Del Pozo, Biomechanical Remodeling of the
597 Microenvironment by Stromal Caveolin-1 Favors Tumor Invasion and Metastasis, Cell. 146
598 (2011) 148–163. doi:10.1016/j.cell.2011.05.040.
- 599 [11] B. Erdogan, M. Ao, L.M. White, A.L. Means, B.M. Brewer, L. Yang, M.K. Washington, C. Shi,
600 O.E. Franco, A.M. Weaver, S.W. Hayward, D. Li, D.J. Webb, Cancer-associated fibroblasts
601 promote directional cancer cell migration by aligning fibronectin, J. Cell Biol. (2017)
602 jcb.201704053. doi:10.1083/jcb.201704053.
- 603 [12] J. Stanisavljevic, J. Loubat-Casanovas, M. Herrera, T. Luque, R. Pena, A. Lluch, J. Albanell, F.
604 Bonilla, A. Rovira, C. Pena, D. Navajas, F. Rojo, A. Garcia de Herreros, J. Baulida, Snail1-
605 Expressing Fibroblasts in the Tumor Microenvironment Display Mechanical Properties That
606 Support Metastasis, Cancer Res. 75 (2015) 284–295. doi:10.1158/0008-5472.CAN-14-1903.
- 607 [13] S. Sakai, C. Iwata, H.Y. Tanaka, H. Cabral, Y. Morishita, K. Miyazono, M.R. Kano, Increased
608 fibrosis and impaired intratumoral accumulation of macromolecules in a murine model of
609 pancreatic cancer co-administered with FGF-2, J. Control. Release. 230 (2016) 109–115.
610 doi:10.1016/j.jconrel.2016.04.007.
- 611 [14] P.P. Provenzano, C. Cuevas, A.E. Chang, V.K. Goel, D.D. Von Hoff, S.R. Hingorani, Enzymatic
612 Targeting of the Stroma Ablates Physical Barriers to Treatment of Pancreatic Ductal
613 Adenocarcinoma, Cancer Cell. 21 (2012) 418–429. doi:10.1016/j.ccr.2012.01.007.
- 614 [15] M.A. Jacobetz, D.S. Chan, A. Neesse, T.E. Bapiro, N. Cook, K.K. Frese, C. Feig, T. Nakagawa,
615 M.E. Caldwell, H.I. Zecchini, M.P. Lolkema, P. Jiang, A. Kultti, C.B. Thompson, D.C. Maneval,

616 D.I. Jodrell, G.I. Frost, H.M. Shepard, J.N. Skepper, D.A. Tuveson, Hyaluronan impairs vascular
617 function and drug delivery in a mouse model of pancreatic cancer., *Gut*. 62 (2013) 112–20.
618 doi:10.1136/gutjnl-2012-302529.

619 [16] K.P. Olive, M.A. Jacobetz, C.J. Davidson, A. Gopinathan, D. McIntyre, D. Honess, B. Madhu,
620 M.A. Goldgraben, M.E. Caldwell, D. Allard, K.K. Frese, G. Denicola, C. Feig, C. Combs, S.P.
621 Winter, H. Ireland-Zecchini, S. Reichelt, W.J. Howat, A. Chang, M. Dhara, L. Wang, F. Rückert,
622 R. Grützmann, C. Pilarsky, K. Izeradjene, S.R. Hingorani, P. Huang, S.E. Davies, W. Plunkett,
623 M. Egorin, R.H. Hruban, N. Whitebread, K. McGovern, J. Adams, C. Iacobuzio-Donahue, J.
624 Griffiths, D.A. Tuveson, F. Ruckert, R. Grutzmann, C. Pilarsky, K. Izeradjene, S.R. Hingorani, P.
625 Huang, S.E. Davies, W. Plunkett, M. Egorin, R.H. Hruban, N. Whitebread, K. McGovern, J.
626 Adams, C. Iacobuzio-Donahue, J. Griffiths, D.A. Tuveson, F. Rückert, R. Grützmann, C.
627 Pilarsky, K. Izeradjene, S.R. Hingorani, P. Huang, S.E. Davies, W. Plunkett, M. Egorin, R.H.
628 Hruban, N. Whitebread, K. McGovern, J. Adams, C. Iacobuzio-Donahue, J. Griffiths, D.A.
629 Tuveson, F. Ruckert, R. Grutzmann, C. Pilarsky, K. Izeradjene, S.R. Hingorani, P. Huang, S.E.
630 Davies, W. Plunkett, M. Egorin, R.H. Hruban, N. Whitebread, K. McGovern, J. Adams, C.
631 Iacobuzio-Donahue, J. Griffiths, D.A. Tuveson, Inhibition of Hedgehog signaling enhances
632 delivery of chemotherapy in a mouse model of pancreatic cancer., *Science*. 324 (2009) 1457–61.
633 doi:10.1126/science.1171362.

634 [17] A.D. Rhim, P.E. Oberstein, D.H. Thomas, E.T. Mirek, C.F. Palermo, S.A. Sastra, E.N. Dekleva,
635 T. Saunders, C.P. Becerra, I.W. Tattersall, C.B. Westphalen, J. Kitajewski, M.G. Fernandez-
636 Barrena, M.E. Fernandez-Zapico, C. Iacobuzio-Donahue, K.P. Olive, B.Z. Stanger, Stromal
637 elements act to restrain, rather than support, pancreatic ductal adenocarcinoma., *Cancer Cell*. 25
638 (2014) 735–47. doi:10.1016/j.ccr.2014.04.021.

639 [18] B.C. Özdemir, T. Pentcheva-Hoang, J.L. Carstens, X. Zheng, C.-C. Wu, T.R. Simpson, H. Laklai,

640 H. Sugimoto, C. Kahlert, S. V. Novitskiy, A. De Jesus-Acosta, P. Sharma, P. Heidari, U.
641 Mahmood, L. Chin, H.L. Moses, V.M. Weaver, A. Maitra, J.P. Allison, V.S. LeBleu, R. Kalluri,
642 Depletion of carcinoma-associated fibroblasts and fibrosis induces immunosuppression and
643 accelerates pancreas cancer with reduced survival., *Cancer Cell*. 25 (2014) 719–734.
644 doi:10.1016/j.ccr.2014.04.005.

645 [19] J.J. Lee, R.M. Perera, H. Wang, D.-C. Wu, X.S. Liu, S. Han, J. Fitamant, P.D. Jones, K.S.
646 Ghanta, S. Kawano, J.M. Nagle, V. Deshpande, Y. Boucher, T. Kato, J.K. Chen, J.K. Willmann,
647 N. Bardeesy, P.A. Beachy, Stromal response to Hedgehog signaling restrains pancreatic cancer
648 progression, *Proc. Natl. Acad. Sci.* 111 (2014) E3091–E3100. doi:10.1073/pnas.1411679111.

649 [20] M.H. Sherman, R.T. Yu, D.D. Engle, N. Ding, A.R. Atkins, H. Tiriach, E.A. Collisson, F. Connor,
650 T. Van Dyke, S. Kozlov, P. Martin, T.W. Tseng, D.W. Dawson, T.R. Donahue, A. Masamune, T.
651 Shimosegawa, M. V Apte, J.S. Wilson, B. Ng, S.L. Lau, J.E. Gunton, G.M. Wahl, T. Hunter, J.A.
652 Drebin, P.J. O’Dwyer, C. Liddle, D.A. Tuveson, M. Downes, R.M. Evans, Vitamin D receptor-
653 mediated stromal reprogramming suppresses pancreatitis and enhances pancreatic cancer
654 therapy., *Cell*. 159 (2014) 80–93. doi:10.1016/j.cell.2014.08.007.

655 [21] A. Chronopoulos, B. Robinson, M. Sarper, E. Cortes, V. Auernheimer, D. Lachowski, S.
656 Attwood, R. García, S. Ghassemi, B. Fabry, A. Del Río Hernández, ATRA mechanically
657 reprograms pancreatic stellate cells to suppress matrix remodelling and inhibit cancer cell
658 invasion., *Nat. Commun.* 7 (2016) 12630. doi:10.1038/ncomms12630.

659 [22] A.A. Rucki, Pancreatic cancer stroma: Understanding biology leads to new therapeutic strategies,
660 *World J. Gastroenterol.* 20 (2014) 2237. doi:10.3748/wjg.v20.i9.2237.

661 [23] H.Y. Tanaka, M.R. Kano, Stromal barriers to nanomedicine penetration in the pancreatic tumor
662 microenvironment, *Cancer Sci.* 109 (2018) 2085–2092. doi:10.1111/cas.13630.

663 [24] M.D. Amatangelo, D.E. Bassi, A.J.P. Klein-Szanto, E. Cukierman, Stroma-Derived Three-

664 Dimensional Matrices Are Necessary and Sufficient to Promote Desmoplastic Differentiation of
665 Normal Fibroblasts, *Am. J. Pathol.* 167 (2005) 475–488. doi:10.1016/S0002-9440(10)62991-4.

666 [25] J. Franco-Barraza, D.A. Beacham, M.D. Amatangelo, E. Cukierman, Preparation of Extracellular
667 Matrices Produced by Cultured and Primary Fibroblasts, in: *Curr. Protoc. Cell Biol.*, John Wiley
668 & Sons, Inc., Hoboken, NJ, USA, 2016: p. 10.9.1-10.9.34. doi:10.1002/cpcb.2.

669 [26] H.-O. Lee, S.R. Mullins, J. Franco-Barraza, M. Valianou, E. Cukierman, J.D. Cheng, FAP-
670 overexpressing fibroblasts produce an extracellular matrix that enhances invasive velocity and
671 directionality of pancreatic cancer cells, *BMC Cancer.* 11 (2011) 245. doi:10.1186/1471-2407-11-
672 245.

673 [27] C.R. Drifka, K.W. Eliceiri, S.M. Weber, W.J. Kao, A bioengineered heterotypic stroma-cancer
674 microenvironment model to study pancreatic ductal adenocarcinoma., *Lab Chip.* 13 (2013) 3965–
675 75. doi:10.1039/c3lc50487e.

676 [28] M. Matsusaki, M. Komeda, S. Mura, H.Y. Tanaka, M.R. Kano, P. Couvreur, M. Akashi,
677 Desmoplastic Reaction in 3D-Pancreatic Cancer Tissues Suppresses Molecular Permeability,
678 *Adv. Healthc. Mater.* 6 (2017) 1700057. doi:10.1002/adhm.201700057.

679 [29] I. Serebriiskii, R. Castelló-Cros, A. Lamb, E.A. Golemis, E. Cukierman, Fibroblast-derived 3D
680 matrix differentially regulates the growth and drug-responsiveness of human cancer cells, *Matrix*
681 *Biol.* 27 (2008) 573–585. doi:10.1016/j.matbio.2008.02.008.

682 [30] E. Karnevi, A.H. Rosendahl, K.S. Hilmersson, M.A. Saleem, R. Andersson, Impact by pancreatic
683 stellate cells on epithelial-mesenchymal transition and pancreatic cancer cell invasion: Adding a
684 third dimension in vitro, *Exp. Cell Res.* 346 (2016) 206–215. doi:10.1016/j.yexcr.2016.07.017.

685 [31] H. Hosoya, K. Kadowaki, M. Matsusaki, H. Cabral, H. Nishihara, H. Ijichi, K. Koike, K.
686 Kataoka, K. Miyazono, M. Akashi, M.R. Kano, Engineering fibrotic tissue in pancreatic cancer:
687 A novel three-dimensional model to investigate nanoparticle delivery, *Biochem. Biophys. Res.*

688 Commun. 419 (2012) 32–37. doi:10.1016/j.bbrc.2012.01.117.

689 [32] D.L. Priwitaningrum, J.-B.G. Blondé, A. Sridhar, J. van Baarlen, W.E. Hennink, G. Storm, S. Le
690 Gac, J. Prakash, Tumor stroma-containing 3D spheroid arrays: A tool to study nanoparticle
691 penetration, *J. Control. Release.* 244 (2016) 257–268. doi:10.1016/j.jconrel.2016.09.004.

692 [33] J. Yu, M.M. Seldin, K. Fu, S. Li, L. Lam, P. Wang, Y. Wang, D. Huang, T.L. Nguyen, B. Wei,
693 R.P. Kulkarni, D. Di Carlo, M. Teitell, M. Pellegrini, A.J. Lusic, A. Deb, Topological
694 Arrangement of Cardiac Fibroblasts Regulates Cellular Plasticity, *Circ. Res.* 123 (2018) 73–85.
695 doi:10.1161/CIRCRESAHA.118.312589.

696 [34] X. Cui, Y. Hartanto, H. Zhang, Advances in multicellular spheroids formation., *J. R. Soc.*
697 *Interface.* 14 (2017). doi:10.1098/rsif.2016.0877.

698 [35] A.D. Bradshaw, The role of SPARC in extracellular matrix assembly., *J. Cell Commun. Signal.* 3
699 (2009) 239–46. doi:10.1007/s12079-009-0062-6.

700 [36] C. Neuzillet, A. Tijeras-Raballand, J. Cros, S. Faivre, P. Hammel, E. Raymond, Stromal
701 expression of SPARC in pancreatic adenocarcinoma., *Cancer Metastasis Rev.* 32 (2013) 585–602.
702 doi:10.1007/s10555-013-9439-3.

703 [37] J. Vaz, D. Ansari, A. Sasor, R. Andersson, SPARC: A Potential Prognostic and Therapeutic
704 Target in Pancreatic Cancer., *Pancreas.* 44 (2015) 1024–1035.
705 doi:10.1097/MPA.0000000000000409.

706 [38] J.R. Infante, H. Matsubayashi, N. Sato, J. Tonascia, A.P. Klein, T.A. Riall, C. Yeo, C. Iacobuzio-
707 Donahue, M. Goggins, Peritumoral fibroblast SPARC expression and patient outcome with
708 resectable pancreatic adenocarcinoma, *J. Clin. Oncol.* 25 (2007) 319–25.
709 doi:10.1200/JCO.2006.07.8824.

710 [39] R.A. Moffitt, R. Marayati, E.L. Flate, K.E. Volmar, S.G.H. Loeza, K.A. Hoadley, N.U. Rashid,
711 L.A. Williams, S.C. Eaton, A.H. Chung, J.K. Smyla, J.M. Anderson, H.J. Kim, D.J. Bentrem,

712 M.S. Talamonti, C.A. Iacobuzio-Donahue, M.A. Hollingsworth, J.J. Yeh, Virtual microdissection
713 identifies distinct tumor- and stroma-specific subtypes of pancreatic ductal adenocarcinoma, *Nat.*
714 *Genet.* 47 (2015) 1168–1178. doi:10.1038/ng.3398.

715 [40] S. Yuzawa, M.R. Kano, T. Einama, H. Nishihara, PDGFR β expression in tumor stroma of
716 pancreatic adenocarcinoma as a reliable prognostic marker., *Med. Oncol.* 29 (2012) 2824–30.
717 doi:10.1007/s12032-012-0193-0.

718 [41] H. Nishihara, Human pathological basis of blood vessels and stromal tissue for nanotechnology.,
719 *Adv. Drug Deliv. Rev.* 74 (2014) 19–27. doi:10.1016/j.addr.2014.01.005.

720 [42] A. Masamune, K. Kikuta, T. Watanabe, K. Satoh, M. Hirota, S. Hamada, T. Shimosegawa,
721 Fibrinogen induces cytokine and collagen production in pancreatic stellate cells, *Gut.* 58 (2009)
722 550–559. doi:10.1136/gut.2008.154401.

723 [43] S. Hamada, A. Masamune, T. Takikawa, N. Suzuki, K. Kikuta, M. Hirota, H. Hamada, M.
724 Kobune, K. Satoh, T. Shimosegawa, Pancreatic stellate cells enhance stem cell-like phenotypes in
725 pancreatic cancer cells, *Biochem. Biophys. Res. Commun.* 421 (2012) 349–354.
726 doi:10.1016/j.bbrc.2012.04.014.

727 [44] R. Rezakhaniha, A. Ajianniotis, J.T.C. Schrauwen, A. Griffa, D. Sage, C.V.C. Bouten, F.N. van
728 de Vosse, M. Unser, N. Stergiopoulos, Experimental investigation of collagen waviness and
729 orientation in the arterial adventitia using confocal laser scanning microscopy, *Biomech. Model.*
730 *Mechanobiol.* 11 (2012) 461–473. doi:10.1007/s10237-011-0325-z.

731 [45] H. Laklai, Y.A. Miroshnikova, M.W. Pickup, E.A. Collisson, G.E. Kim, A.S. Barrett, R.C. Hill,
732 J.N. Lakins, D.D. Schlaepfer, J.K. Mouw, V.S. LeBleu, N. Roy, S. V. Novitskiy, J.S. Johansen,
733 V. Poli, R. Kalluri, C.A. Iacobuzio-Donahue, L.D. Wood, M. Hebrok, K. Hansen, H.L. Moses,
734 V.M. Weaver, Genotype tunes pancreatic ductal adenocarcinoma tissue tension to induce
735 matricellular fibrosis and tumor progression, *Nat. Med.* 22 (2016) 497–505.

736 doi:10.1038/nm.4082.

737 [46] J. Haqq, L.M. Howells, G. Garcea, M.S. Metcalfe, W.P. Steward, A.R. Dennison, Pancreatic
738 stellate cells and pancreas cancer: current perspectives and future strategies., *Eur. J. Cancer.* 50
739 (2014) 2570–82. doi:10.1016/j.ejca.2014.06.021.

740 [47] A. Nesses, H. Algül, D.A. Tuveson, T.M. Gress, Stromal biology and therapy in pancreatic
741 cancer: a changing paradigm, *Gut.* 64 (2015) 1476–1484. doi:10.1136/gutjnl-2015-309304.

742 [48] A. Moustakas, C.-H. Heldin, Non-Smad TGF- signals, *J. Cell Sci.* 118 (2005) 3573–3584.
743 doi:10.1242/jcs.02554.

744 [49] C.J. Whatcott, S. Ng, M.T. Barrett, G. Hostetter, D.D. Von Hoff, H. Han, Inhibition of ROCK1
745 kinase modulates both tumor cells and stromal fibroblasts in pancreatic cancer, *PLoS One.* 12
746 (2017) e0183871. doi:10.1371/journal.pone.0183871.

747 [50] A. Masamune, K. Kikuta, M. Satoh, K. Satoh, T. Shimosegawa, Rho kinase inhibitors block
748 activation of pancreatic stellate cells, *Br. J. Pharmacol.* 140 (2003) 1292–1302.
749 doi:10.1038/sj.bjp.0705551.

750 [51] K. Kessenbrock, V. Plaks, Z. Werb, Matrix Metalloproteinases: Regulators of the Tumor
751 Microenvironment, *Cell.* 141 (2010) 52–67. doi:10.1016/j.cell.2010.03.015.

752 [52] P.A. Phillips, J.A. McCarroll, S. Park, M.-J. Wu, R. Pirola, M. Korsten, J.S. Wilson, M. V Apte,
753 Rat pancreatic stellate cells secrete matrix metalloproteinases: implications for extracellular
754 matrix turnover., *Gut.* 52 (2003) 275–82. <http://www.ncbi.nlm.nih.gov/pubmed/12524413>.

755 [53] W. Schneiderhan, F. Diaz, M. Fundel, S. Zhou, M. Siech, C. Hasel, P. Moller, J.E. Gschwend, T.
756 Seufferlein, T. Gress, G. Adler, M.G. Bachem, Pancreatic stellate cells are an important source of
757 MMP-2 in human pancreatic cancer and accelerate tumor progression in a murine xenograft
758 model and CAM assay, *J. Cell Sci.* 120 (2007) 512–519. doi:10.1242/jcs.03347.

759 [54] R. Vishnubhotla, S. Sun, J. Huq, M. Bulic, A. Ramesh, G. Guzman, M. Cho, S.C. Glover, ROCK-

760 II mediates colon cancer invasion via regulation of MMP-2 and MMP-13 at the site of
761 invadopodia as revealed by multiphoton imaging., *Lab. Invest.* 87 (2007) 1149–58.
762 doi:10.1038/labinvest.3700674.

763 [55] M. Li, Z. Li, X. Sun, Statins suppress MMP2 secretion via inactivation of RhoA/ROCK pathway
764 in pulmonary vascular smooth muscles cells., *Eur. J. Pharmacol.* 591 (2008) 219–23.
765 doi:10.1016/j.ejphar.2008.06.082.

766 [56] F. Xue, T. Takahara, Y. Yata, Q. Xia, K. Nonome, E. Shinno, M. Kanayama, S. Takahara, T.
767 Sugiyama, Blockade of Rho/Rho-associated coiled coil-forming kinase signaling can prevent
768 progression of hepatocellular carcinoma in matrix metalloproteinase-dependent manner., *Hepatol.*
769 *Res.* 38 (2008) 810–7. doi:10.1111/j.1872-034X.2008.00333.x.

770 [57] I. Abécassis, B. Olofsson, M. Schmid, G. Zalzman, A. Karniguian, RhoA induces MMP-9
771 expression at CD44 lamellipodial focal complexes and promotes HMEC-1 cell invasion., *Exp.*
772 *Cell Res.* 291 (2003) 363–76. <http://www.ncbi.nlm.nih.gov/pubmed/14644158>.

773 [58] A. Francki, A.D. Bradshaw, J.A. Bassuk, C.C. Howe, W.G. Couser, E.H. Sage, SPARC regulates
774 the expression of collagen type I and transforming growth factor-beta1 in mesangial cells., *J.*
775 *Biol. Chem.* 274 (1999) 32145–52. doi:10.1074/jbc.274.45.32145.

776 [59] K.M. Yamada, E. Cukierman, Modeling Tissue Morphogenesis and Cancer in 3D, *Cell.* 130
777 (2007) 601–610. doi:10.1016/j.cell.2007.08.006.

778 [60] M. Matsusaki, C.P. Case, M. Akashi, Three-dimensional cell culture technique and
779 pathophysiology, *Adv. Drug Deliv. Rev.* 74 (2014) 95–103. doi:10.1016/j.addr.2014.01.003.

780 [61] E. Brown, T. McKee, E. DiTomaso, A. Pluen, B. Seed, Y. Boucher, R.K. Jain, Dynamic imaging
781 of collagen and its modulation in tumors in vivo using second-harmonic generation, *Nat. Med.* 9
782 (2003) 796–801. doi:10.1038/nm879.

783 [62] G. Cox, E. Kable, A. Jones, I. Fraser, F. Manconi, M.D. Gorrell, 3-Dimensional imaging of

784 collagen using second harmonic generation, *J. Struct. Biol.* 141 (2003) 53–62.
785 doi:10.1016/S1047-8477(02)00576-2.

786 [63] R.M. Williams, W.R. Zipfel, W.W. Webb, Interpreting Second-Harmonic Generation Images of
787 Collagen I Fibrils, *Biophys. J.* 88 (2005) 1377–1386. doi:10.1529/biophysj.104.047308.

788 [64] F.H. Epstein, W.A. Border, N.A. Noble, Transforming Growth Factor β in Tissue Fibrosis, *N.*
789 *Engl. J. Med.* 331 (1994) 1286–1292. doi:10.1056/NEJM199411103311907.

790 [65] K. Zhang, W.R. Grither, S. Van Hove, H. Biswas, S.M. Ponik, K.W. Eliceiri, P.J. Keely, G.D.
791 Longmore, Mechanical signals regulate and activate SNAIL1 protein to control the fibrogenic
792 response of cancer-associated fibroblasts, *J. Cell Sci.* 129 (2016) 1989–2002.
793 doi:10.1242/jcs.180539.

794 [66] S. Neri, G. Ishii, H. Hashimoto, T. Kuwata, K. Nagai, H. Date, A. Ochiai, Podoplanin-expressing
795 cancer-associated fibroblasts lead and enhance the local invasion of cancer cells in lung
796 adenocarcinoma., *Int. J. Cancer.* 137 (2015) 784–96. doi:10.1002/ijc.29464.

797 [67] F. Calvo, N. Ege, A. Grande-Garcia, S. Hooper, R.P. Jenkins, S.I. Chaudhry, K. Harrington, P.
798 Williamson, E. Moendarbary, G. Charras, E. Sahai, Mechanotransduction and YAP-dependent
799 matrix remodelling is required for the generation and maintenance of cancer-associated
800 fibroblasts, *Nat. Cell Biol.* 15 (2013) 637–646. doi:10.1038/ncb2756.

801 [68] G. Chen, X. Tian, Z. Liu, S. Zhou, B. Schmidt, D. Henne-Bruns, M. Bachem, M. Kornmann,
802 Inhibition of endogenous SPARC enhances pancreatic cancer cell growth: modulation by FGFR1-
803 III isoform expression., *Br. J. Cancer.* 102 (2010) 188–195. doi:10.1038/sj.bjc.6605440.

804 [69] M. Hidalgo, C. Plaza, M. Musteanu, P. Illei, C.B. Brachmann, C. Heise, D. Pierce, P.P. Lopez-
805 Casas, C. Menendez, J. Taberero, A. Romano, X. Wei, F. Lopez-Rios, D.D. Von Hoff, SPARC
806 Expression Did Not Predict Efficacy of nab-Paclitaxel plus Gemcitabine or Gemcitabine Alone
807 for Metastatic Pancreatic Cancer in an Exploratory Analysis of the Phase III MPACT Trial, *Clin.*

808 Cancer Res. 21 (2015) 4811–4818. doi:10.1158/1078-0432.CCR-14-3222.

809 [70] H. Kim, S. Samuel, P. Lopez-Casas, W. Grizzle, M. Hidalgo, J. Kovar, D. Oelschlager, K. Zinn,
810 J. Warram, D. Buchsbaum, SPARC-Independent Delivery of Nab-Paclitaxel without Depleting
811 Tumor Stroma in Patient-Derived Pancreatic Cancer Xenografts., *Mol. Cancer Ther.* 15 (2016)
812 680–8. doi:10.1158/1535-7163.MCT-15-0764.

813 [71] D.D. Von Hoff, R.K. Ramanathan, M.J. Borad, D.A. Laheru, L.S. Smith, T.E. Wood, R.L. Korn,
814 N. Desai, V. Trieu, J.L. Iglesias, H. Zhang, P. Soon-Shiong, T. Shi, N.V. V Rajeshkumar, A.
815 Maitra, M. Hidalgo, Gemcitabine Plus nab -Paclitaxel Is an Active Regimen in Patients With
816 Advanced Pancreatic Cancer: A Phase I/II Trial, *J. Clin. Oncol.* 29 (2011) 4548–54.
817 doi:10.1200/JCO.2011.36.5742.

818 [72] A.D. Bradshaw, P. Puolakkainen, J. Dasgupta, J.M. Davidson, T.N. Wight, E. Helene Sage, E.H.
819 Sage, SPARC-null mice display abnormalities in the dermis characterized by decreased collagen
820 fibril diameter and reduced tensile strength, *J. Invest. Dermatol.* 120 (2003) 949–55.
821 doi:10.1046/j.1523-1747.2003.12241.x.

822 [73] F. Di Maggio, P. Arumugam, F.R. Delvecchio, S. Batista, T. Lechertier, K. Hodivala-Dilke, H.M.
823 Kocher, Pancreatic stellate cells regulate blood vessel density in the stroma of pancreatic ductal
824 adenocarcinoma, *Pancreatology.* 16 (2016) 995–1004. doi:10.1016/j.pan.2016.05.393.

825 [74] E.F. Carapuça, E. Gemenetzidis, C. Feig, T.E. Bapiro, M.D. Williams, A.S. Wilson, F.R.
826 Delvecchio, P. Arumugam, R.P. Grose, N.R. Lemoine, F.M. Richards, H.M. Kocher, Anti-
827 stromal treatment together with chemotherapy targets multiple signalling pathways in pancreatic
828 adenocarcinoma, *J. Pathol.* 239 (2016) 286–296. doi:10.1002/path.4727.

829 [75] S.F. Boj, C.-I. Hwang, L.A. Baker, I.I.C. Chio, D.D. Engle, V. Corbo, M. Jager, M. Ponz-Sarvise,
830 H. Tiriác, M.S. Spector, A. Gracanin, T. Oni, K.H. Yu, R. van Boxtel, M. Huch, K.D. Rivera, J.P.
831 Wilson, M.E. Feigin, D. Öhlund, A. Handly-Santana, C.M. Ardito-Abraham, M. Ludwig, E.

832 Elyada, B. Alagesan, G. Biffi, G.N. Yordanov, B. Delcuze, B. Creighton, K. Wright, Y. Park,
833 F.H.M. Morsink, I.Q. Molenaar, I.H. Borel Rinkes, E. Cuppen, Y. Hao, Y. Jin, I.J. Nijman, C.
834 Iacobuzio-Donahue, S.D. Leach, D.J. Pappin, M. Hammell, D.S. Klimstra, O. Basturk, R.H.
835 Hruban, G.J. Offerhaus, R.G.J. Vries, H. Clevers, D.A. Tuveson, Organoid Models of Human and
836 Mouse Ductal Pancreatic Cancer, *Cell*. 160 (2015) 324–338. doi:10.1016/j.cell.2014.12.021.
837 [76] M.J. Ware, V. Keshishian, J.J. Law, J.C. Ho, C.A. Favela, P. Rees, B. Smith, S. Mohammad, R.F.
838 Hwang, K. Rajapakshe, C. Coarfa, S. Huang, D.P. Edwards, S.J. Corr, B. Godin, S.A. Curley,
839 Generation of an in vitro 3D PDAC stroma rich spheroid model, *Biomaterials*. 108 (2016) 129–
840 142. doi:10.1016/j.biomaterials.2016.08.041.
841 [77] J. Haqq, L.M. Howells, G. Garcea, A.R. Dennison, Targeting pancreatic cancer using a
842 combination of gemcitabine with the omega-3 polyunsaturated fatty acid emulsion, *Lipidem*TM,
843 *Mol. Nutr. Food Res.* 60 (2016) 1437–1447. doi:10.1002/mnfr.201500755.
844 [78] F. Grinnell, H. Fukamizu, P. Pawelek, S. Nakagawa, Collagen processing, crosslinking, and fibril
845 bundle assembly in matrix produced by fibroblasts in long-term cultures supplemented with
846 ascorbic acid., *Exp. Cell Res.* 181 (1989) 483–91.
847 <http://www.ncbi.nlm.nih.gov/pubmed/2924799>.
848